OFFICE OF NAVAL RESEARCH
Contract N00014-91-J-1045
R&T Code 4132047--02-1

TECHNICAL REPORT NO. 7

The Control of Gas Transport in Heterogeneous Polymer Systems

by

D.H. Rein, R.F. Baddour and R.E. Cohen
Department of Chemical Engineering
Massachusetts Institute of Technology
Cambridge, MA 02139-4307

October 18, 1991

DISCLAIMER NOTICE

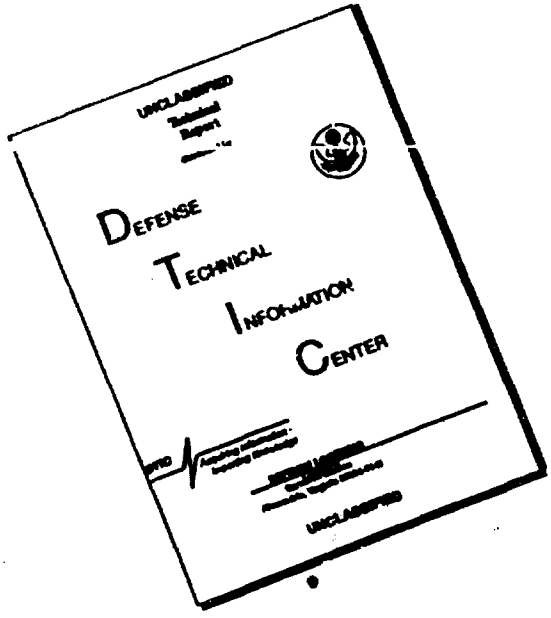

THIS DOCUMENT IS BEST QUALITY AVAILABLE. THE COPY FURNISHED TO DTIC CONTAINED A SIGNIFICANT NUMBER OF PAGES WHICH DO NOT REPRODUCE LEGIBLY.

SECURITY CLASSIFICATION OF THIS PAGE

REPORT DOCUMENTATION PAGE

1a. REPORT SECURITY CLASSIFICATION	1b. RESTRICTIVE MARKINGS
2a. SECURITY CLASSIFICATION AUTHORITY	3. DISTRIBUTION / AVAILABILITY OF REPORT
2b. DECLASSIFICATION / DOWNGRADING SCHEDULE	unlimited
4. PERFORMING ORGANIZATION REPORT NUMBER(S)	5. MONITORING ORGANIZATION REPORT NUMBER(S)
Technical Report No. 7	

6a. NAME OF PERFORMING ORGANIZATION	6b. OFFICE SYMBOL (If applicable)	7a. NAME OF MONITORING ORGANIZATION	
M.I.T.		ONR	
6c. ADDRESS (City, State, and ZIP Code)		7b. ADDRESS (City, State, and ZIP Code)	
Department of Chemical Engineering Cambridge, MA 02139		800 N. Quincy Street Arlington, VA 22217	
8a. NAME OF FUNDING / SPONSORING ORGANIZATION	8b. OFFICE SYMBOL (If applicable)	9. PROCUREMENT INSTRUMENT IDENTIFICATION NUMBER	
ONR		Noo o14-91-J-1045	
8c. ADDRESS (City, State, and ZIP Code)		10. SOURCE OF FUNDING NUMBERS	
		PROGRAM ELEMENT NO.	PROJECT NO. 4132047
800 N. Quincy Street Arlington, VA 22217			TASK NO. 02
			WORK UNIT ACCESSION NO 1

11. TITLE (Include Security Classification)

Control of Gas Transport in Heterogeneous Polymer Systems

12. PERSONAL AUTHOR(S)

D.H Rein, R.F. Baddour, R.E. Cohen

13a. TYPE OF REPORT	13b. TIME COVERED	14. DATE OF REPORT (Year, Month, Day)	15. PAGE COUNT
Technical	FROM _____ TO _____	October 18,1991	45

16. SUPPLEMENTARY NOTATION

Edited condensation of doctoral thesis of D.H. Rein

17. COSATI CODES			18. SUBJECT TERMS (Continue on reverse if necessary and identify by block number)
FIELD	GROUP	SUB-GROUP	gas barrier materials
			gas transport membranes
			gas separations block copolymers

19. ABSTRACT (Continue on reverse if necessary and identify by block number)

This report focuses on control of gas transport using heterogeneous polymer systems with well-characterized morphologies. Chapters of the report describe chain mobility and restrictions on gas transport, a correlation of gas solubility with glassy polymer enthalpy, gas transport in skin-core membranes and the permeation of gases in a novel microporous block copolymer membrane.

20. DISTRIBUTION / AVAILABILITY OF ABSTRACT	21. ABSTRACT SECURITY CLASSIFICATION
☒ UNCLASSIFIED/UNLIMITED ☐ SAME AS RPT. ☐ DTIC USERS	unlimited

22a. NAME OF RESPONSIBLE INDIVIDUAL	22b. TELEPHONE (Include Area Code)	22c. OFFICE SYMBOL

DD FORM 1473, 84 MAR 83 APR edition may be used until exhausted. All other editions are obsolete.

SECURITY CLASSIFICATION OF THIS PAGE

Table of Contents

List of Figures and Tables

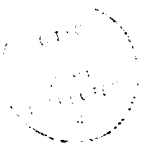

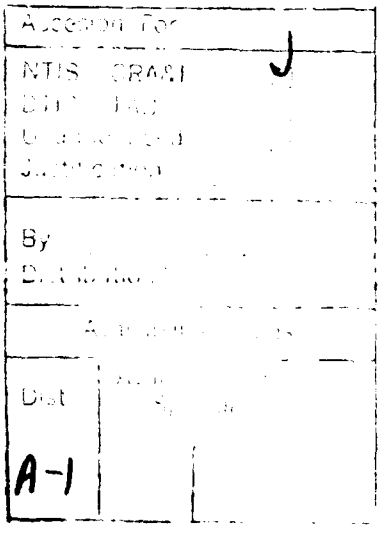

I. Introduction

Polymeric materials have experienced tremendous growth in many gas transport applications including membranes for gas separations and barriers for the packaging industries. In order to meet the increasing demand for new applications, an understanding of the role of molecular architecture and supermolecular structure on the gas transport is essential. These structure / property relationships will help to explain, for example, the extraordinary behavior of polymers such as poly(1-(trimethylsilyl)-1-propyne), a new glassy polymer that exhibits gas permeabilities a factor of ten higher than any other polymer studied as well as speed the development of others [1].

Control over gas transport is possible through the use of multicomponent heterogeneous polymer systems. Among the features in these systems which affect small molecule transport are the size, shape and orientation of the (micro)phase separated morphology, the high internal surface / volume ratio and the diffuse interfacial regions. For instance, a block copolymer with spherical microphase separation has gas transport properties vastly different from those of the same copolymer with lamellar microphase separation. Similarly, the gas transport properties in a block copolymer with oriented lamellae are strongly dependent on the direction of diffusion. Heterogeneous polymer systems provide the opportunity to molecularly engineer a membrane with the structural characteristics of one component and the transport behavior of the other component, creating a new material with mechanical and transport properties superior to those of the parent homopolymers. However, successful manufacturing and usage of these heterogeneous polymers demands knowledge of the relationships between the morphology and the diffusion and permeation processes.

Such structure / property relationships can be obtained by a combination of diffusional studies and detailed morphological investigation. In addition to providing transport parameters, diffusion studies can provide information about the internal structure and chain behavior not accessible from conventional morphological characterization techniques such as transmission electron microscopy (TEM) and small angle x-ray scattering (SAXS). Chain immobilization, relaxation kinetics and diffuse interfacial regions have been investigated using transport analyses [2-6]. Few studies exist, however, which have combined measurements of transport properties with detailed morphological information, and these have been complicated by domain structures with random macroscopic orientation.

This work focuses on the control of gas transport using heterogeneous polymer systems with well defined morphology. Two areas of gas transport are addressed: 1) characterizing polymer chain dynamics and enthalpy states discernible from the transport behavior of penetrant gas probes and 2) exploring two modification techniques to alter gas transport using heterogeneous polymers. The digest is organized into four remaining chapters. Chapter two describes the sorption apparatus to measure diffusion and solubility coefficients then investigates differences in gas diffusion

between one of the components of a block copolymer and the corresponding homopolymer. In chapter three, the solubilities of penetrant gas probes are used to correlate the different enthalpy states of glassy polystyrenes with a range of molecular weights. Chapter four addresses the morphological and gas transport changes accompanying the bromination of polybutadiene in the solid state. A novel method to create microporous membranes and the effect on gas permeation and diffusion is described in the last chapter.

II. Diffusion and Solubility in a Polystyrene - Polybutadiene Block Copolymer

This chapter investigates the solubility and diffusion coefficients for CO_2, CH_4 and Ar in polystyrene/polybutadiene (SB) block copolymer films measured in a pressure decay sorption apparatus at 1 atm over a temperature range of 20 to 90 °C. Diffusion behavior in the copolymer was simulated using homopolybutadiene and homopolystyrene data along with a finite difference model based on the well-ordered morphology. Comparisons of the model predictions with the measured values of the effective diffusion coefficients for the gases in the copolymer revealed differences in gas transport between the polybutadiene regions of the block copolymer and the corresponding homopolymer.

2.1 Experimental Section

2.1.1 Materials

Polystyrene (S) homopolymer was obtained from Polysciences, Inc., and polybutadiene (B ; 90% 1,4 addition) was obtained from Scientific Polymer Products, Inc; both homopolymers had molecular weights of 200,000 g/mole. Phillips Petroleum Co. supplied a 0.05 cm extruded sheet of an experimental grade of polystyrene-polybutadiene block copolymer (SB) which was part of their K-Resin series. This block copolymer contained 75% (v/v) polystyrene and had a weight average molecular weight of 187,000 g/mol with Mw/Mn = 1.5 [7,8]. The bulk morphology of the material is polybutadiene lamellae (ca. 100 Å thick) with excellent long-range orientation in the extrusion direction as observed via TEM and SAXS experiments. Specimens were prepared [7, 8] from this extruded sheet so that the lamellae were perpendicular to the surfaces of the disk-shaped films placed into the sorption apparatus.

2.1.2 Sorption Apparatus

Figure 2-1 is a schematic diagram of the apparatus used to measure transient sorption. The main components of the system include sample, storage and calibration volumes, a sensitive pressure transducer, and a data acquisition system. Polymer films used in sorption experiments were disk shaped with a radius of 1.25 cm and a thickness of 0.02 - 0.05 cm. After the sample was loaded, a mechanical pump was used to evacuate volume A to about 10^{-2} torr, and the storage volume was filled with the test gas. The polymer was then degassed for at least twice the time required to reach

sorption equilibrium. A sorption run was started by allowing a portion of the test gas into volume A from volume B and simultaneously starting the data acquisition program. The solubility and diffusion coefficients were measured at 1 atm over the temperature range 20 - 90 °C.

A simple and standard model for sorption experiments was used to process the transient pressure decay data [9,10]. The experiment was modeled as one dimensional diffusion into a plane sheet with penetrant entering perpendicular to the plane surfaces. Crank presents several methods to obtain a diffusion coefficient from transient sorption data [9,10]. We employed two of these methods. The initial slope method takes advantage of the small time asymptotic limit of the sorption curve :

$$\frac{M_t}{M_\infty} = 4 \left(\frac{D t}{l^2 \pi} \right)^{0.5} \qquad (1)$$

where M_t is the amount (g) of diffusant in the sheet at time t (sec), M_∞ is the amount of diffusant in the sheet at equilibrium, D is the diffusion coefficient (cm^2/sec), and l is the sheet thickness (cm). The diffusion coefficient is obtained from the slope of the linear portion of a plot of M_t / M_∞ vs $t^{0.5}$. The second method [9,10] uses the half-time ($t_{1/2}$ is the time required to sorb $M_\infty/2$) of the sorption process to calculate the diffusion coefficient.

$$D = \frac{0.05}{t_{1/2} / l^2} \qquad (2)$$

Solubility coefficient, S [cm^3 (STP) / cm^3 / cm Hg], was obtained from the volume of the penetrant absorbed at equilibrium (V_g) , the volume of the polymer sample (V_p) , and the final penetrant pressure (P_{eq})

$$S = \frac{V_g (STP)}{V_p P_{eq}} \qquad (3)$$

where STP indicates standard conditions of 273 K and 1 atm. The volume of the gas absorbed in the polymer was calculated from the number of moles of gas absorbed:

$$V_g (STP) = \frac{22.4 * (P_{in} - P_{eq}) * V_a}{R * T} \qquad (4)$$

The final pressure (P_{eq}) was determined from the pressure transducer reading at sorption equilibrium, and the initial pressure reading (P_{in}) was estimated from an extrapolation of the pressure decay readings.

2.2 Results and Discussion

2.2.1 Transport Results

Figure 2-2 summarizes the temperature dependence of the equilibrium solubility coefficients for CO_2 in B, S, and SB. The heats of solution (kJ/mole) calculated from these plots by a least squares

method were -9, -22, and -15 for B, S, and SB, respectively. The solubility coefficients for Ar and CH_4 showed similar temperature dependences and the heats of solution for the copolymer were bracketed by the homopolymer values. It is of interest to compare the observed block copolymer solubility to that predicted from homopolymer values. The solubility coefficient is an equilibrium property which can be described for a heterogeneous polymer system as a linear combination of the homopolymer values [11]

$$S^* = v_S S_S + v_B S_B \qquad (5)$$

where S_S, and S_B are the solubility coefficients for the pure materials, S* is the solubility coefficient for the composite, and v_S and v_B are the volume fractions in the composite.

Over the temperature range of 20 to 90 °C, the calculated S* values from equation (5) agree to within 10% of the measured S values for the three gases. Thus, the simple two phase model given by equation (5) adequately describes the equilibrium properties of the block copolymer, i.e. the solubility coefficients, over a range of temperatures.

The CO_2 , Ar and CH_4 diffusion coefficients for B, S, and SB were plotted as a function of temperature in an Arrhenius form in Figures 2-3a - 2-3c. The apparent activation energy for diffusion, E^D (kJ/mole), calculated from these plots by a least squares analysis for CO_2 were 19, 28, and 32 for B, S and SB respectively, for Ar they were 18, 25 and 34, while for CH_4 they were 22, 36 and 43. Although the diffusion coefficients for the SB diblock lie between those of the S and B homopolymers, the apparent activation energy for SB is larger than for either of the homopolymers. This surprisingly large temperature dependence of the block copolymer diffusion coefficient was investigated by simulating the measured SB diffusion coefficient based on the behavior of the component homopolymers.

We recall that the analysis used to calculate the D from the transient experiment was formulated for sorption into homogeneous materials and is equal to the steady-state D. The steady-state D for a composite material of sheets in parallel, such as the K-Resin, has been described as a linear combination of the component steady-state diffusion coefficients weighted by their respective volume fractions [10]. Because the K-Resin is a composite, the effective diffusion coefficient, Deff, calculated from equations (2) or (3) is not necessarily equal to the steady-state diffusion coefficient of the material. The Deff calculated for SB from the transient sorption experiment can not be obtained from a linear combination of the homopolymer diffusion coefficients.

2.2.2 Simulation Model

In order to relate the measured K-Resin diffusion coefficient, Deff, to homopolymer values, a computer model was developed to simulate the non steady-state diffusion into a composite medium of well defined structure. The two - dimensional grid used in the model divided the width of the lamellae into discrete steps along the x-axis from $x=x_o$ to $x=x_i$ for B and from $x=x_i$ to $x=x_{nx}$ for S; similarly, the length of the lamellae along the y-axis was discretized from $y=y_o$ to $y=y_{ny}$. The

following assumptions were employed: (i) continuous lamellae connect the film surfaces, (ii) two dimensional diffusion takes place in the x-y plane, (iii) diffusion coefficients are independent of concentration. (iv) the diffusion is Fickian [10], (v) surface concentrations are independent of time and position, (vi) the interfaces between the lamellae are sharp, (vii) gas concentrations, c, in the microphase regions are $c_S = K*c_B$ where K is a partition coefficient equal to the ratio of solubility coefficients, S_S/S_B. The equations to be solved are:

$$\partial c_S/\partial t = D_S(\partial^2 c_S/\partial x^2 + \partial^2 c_S/\partial y^2) \quad (6)$$

$$\partial c_B/\partial t = D_B(\partial^2 c_B/\partial x^2 + \partial^2 c_B/\partial y^2) \quad (7)$$

where S and B denote the continuous lamellae; equations (6) and (7) are subject to boundary conditions

i) $c_S = c_B = 0$	$t=0$
ii) $c_S(y=y_o,t) = c_B(y=y_o,t) = Co$	$t>0$
iii) $\partial c_B/\partial x = 0$	$x=x_o$, all t
iv) $\partial c_S/\partial x = 0$	$x=x_{nx}$, all t
v) $\partial c_S/dy = \partial c_B/dy = 0$	$y=y_{ny}$, all t
vi) $D_S\partial c_S/\partial x = D_B\partial c_B/\partial x$	$x=x_i$, all t

A forward finite difference method [10] was employed to solve the equations (6) and (7) using the measured homopolymer values for D and S from 20 to 90 °C as input.

The transient sorption curves generated by the model were analyzed with the half-time method to yield an effective diffusion coefficient, Deff. Figures 2-4a - 2-4c are Arrhenius plots comparing Deff values calculated from half times of the model response and Deff values obtained from the experimental sorption curves. The model overpredicts the measured Kresin diffusion coefficients for the gases; the amount of overprediction decreases as the temperature approaches the Tg of polystyrene. Because the finite difference model uses homopolymer data as input, the observed discrepancy suggests an additional impedance to gas diffusion in the block copolymer not found in the homopolymers. We will suggest below that this extra resistance to gas flow and its temperature dependence are the causes of the unusually high apparent activation energy for diffusion in the K-Resin which was noted earlier (Figures 2-3a - 2-3c).

A similar phenomenon was observed in the Kresin permeabilities [7,8] which were measured using CO_2 in a variable-volume steady state permeation apparatus. Activation energies for permeation obtained from Arrhenius plots of permeability coefficients in the temperature range 25 - 50 °C for the block copolymer (E^P_{SB}) and the homopolymers (E^P_S, E^P_B) are 19.7, 11.7, and 8.4 kJ/mole, respectively; E^P of the K-Resin is significantly larger than either homopolymer value.

Although a 3 - component model which includes an interfacial zone more completely describes the K-Resin [7], for simplicity here the steady state permeability coefficient will be approximated using a two component parallel model [11]:

$$P_{par} = v_B P_B + v_S P_S \qquad (8a)$$

where P_S, P_B, and P_{par} are the permeability coefficients for polystyrene, polybutadiene, and the parallel composite, respectively. P_S and P_B can be expanded into Arrhenius expressions to consider temperature dependence [12]:

$$P_{par} = v_B P_{o,B} \exp(-E^P_B/RT) + v_S P_{o,S} \exp(-E^P_S/RT) \qquad (8b)$$

The apparent activation energy for the parallel system (E_{par}), i.e. that derived from the slope of an Arrhenius plot, can be obtained from the local derivative $\partial(\ln P_{par})/\partial(1/T)$.

$$E^P_{par} = E^P_B(v_B P_B/(v_B P_B + v_S P_S)) + E^P_S(v_S P_S/((v_B P_B + v_S P_S)) \qquad (9)$$

Equation (9) states that the apparent activation energy for permeation is an average of the homopolymer activation energies weighted by respective fractions of the total flux. Because the polybutadiene is considerably more permeable to CO_2 than polystyrene [7,13], E^P_{par} for this system is dominated by E^P_B and the activation energy for the K-Resin is expected to be close to that for polybutadiene. Using equation (9), the calculated E^P_{par} is 8.8 kJ/mole, which is close to that of homopolybutadiene (8.4 kJ/mole) as expected but significantly lower than the experimental value of E^P_{SB} (19.7 kJ/mole). This observation is consistent with the information from the diffusion studies.

As indicated by the comparison between the measured and simulated diffusion coefficients, gas transport through the copolymer is hindered relative to that predicted from the homopolymer components. A number of workers have attributed similar observations of gas impedance in block copolymers to the influence of the diffuse interfacial region between domains [3,5,6,7]. Small angle neutron scattering and gas permeation experiments have determined the interfacial region in SB to be about 25 Å [7].

The interfacial region was considered to determine whether its presence was sufficient to explain the disagreement between the measured and calculated Deff of the K-Resin. The interfacial region can be treated as a random copolymer varying spatially in composition between boundaries from pure styrene to pure butadiene [7]; the average diffusion coefficient of the interface is bracketed by the homopolystyrene and homopolybutadiene values. As a first consideration, the interfacial diffusion coefficient was assumed equal that for S, thereby maximizing its influence in impeding transport. This analysis effectively creates a new heterogeneous copolymer of 12.5 % B and 87.5 % S. For this limiting case the value of Deff at 293 K generated by the model was $56 * 10^{-8}$ cm^2/sec, a value still significantly larger than the observed value of $44 * 10^{-8}$ cm^2/sec. The diffuse interface therefore does not completely explain the discrepancy between the measured and calculated values of Deff shown in Figures 2-4a - 2-4c.

Interactions between the separate regions of heterogeneous materials have also been proposed to explain unexpected restrictions on gas transport in such materials [2,4,5]. For the case of SB block copolymers, the location of the covalent junction between the polystyrene and polybutadiene blocks in the interfacial zone between the lamellae may reduce chain mobility in the polybutadiene region beyond the interface, thereby decreasing the rate of gas diffusion through the rubbery block analogous to the decrease of gas diffusion observed in polybutadiene crosslinked with electron beam irradiation [8,14]. In the SB block copolymer the restriction on chain mobility, and thus the unexpected retardation of gas diffusion, should disappear as the mobility of the polystyrene block increases, i.e. as the polystyrene glass transition temperature is approached.

2.2.3 Immobilization Factor

In order to account for this chain immobilization of the B regions of the copolymer, we decreased the input values to the computer model for the gas diffusion coefficients of CO_2, Ar and CH_4 in the polybutadiene. The extent of adjustment defined a temperature dependent factor

$$ß = D/D^* \qquad (10)$$

where D is the diffusion coefficient of CO_2, Ar or CH_4 through homopolybutadiene, and D* is the adjusted input value to the model, i.e. the presumed diffusion coefficient of CO_2, Ar or CH_4 through the B block of the SB block copolymer. ß combines contributions to chain immobilization outside the interfacial zone and within the interfacial region into a single parameter which describes the restricted mobility of the entire polybutadiene block of the SB. Michaels and Parker [15] in a study of semicrystalline polyethylene attributed a similar immobilization factor to the crosslinking action of crystallites which restricted the chain mobility in the amorphous phases.

At each temperature, a value of ß was chosen so that the prediction of our model matched the measured value of Deff. Table 2-1 lists ß values at several temperatures which are in reasonable correspondence with the results of Odani et al [5] who calculated values of ß for various gases at a single temperature using a styrene-butadiene block copolymer. The immobilization factors at 25 °C reported by Odani et al were 0.99, 1.3, 1.8, 2.4 and 2.4 for He, Ar, N_2, Kr, and Xe, respectively.

Chain immobilization of and restricted diffusion in the polybutadiene regions of the SB block copolymer is caused by the polystyrene regions and the magnitude of this effect depends on the mobility of the polystyrene. At the lowest temperature of our experiment, the polystyrene chains have the least motion, and immobilize the PB chains to the greatest extent (highest ß). This immobilization is expected to decrease as temperature increases, and it should essentially disappear at the polystyrene Tg. This trend is observed in Table 2-1; ß approaches unity as the temperature approaches the Tg of the polystyrene block.

III. A Correlation of Gas Solubility in Glassy Polymers with Excess Enthalpy

In the following chapter, the solubility coefficients for CO_2, Ar and CH_4 in polystyrene (PS) films with glass transition temperatures (Tg) of 52 to 107 °C were measured over a temperature range of 20 to 90 °C. The observed dependence of gas solubility on Tg was analyzed in terms of enthalpy - temperature relationships for glassy polymers. The solubilities for PS samples with different glass transition temperatures converged when comparisons were made based on states of equal enthalpy instead of the temperature of measurement.

3.1 Theoretical Framework

In this section we provide a theoretical framework in which we can anticipate the experimental observations to be presented below. We make use of the nonequilibrium nature of amorphous polymers below the glass transition temperature and the fact that at a specified cooling rate the amount of undercooling below Tg determines the initial amount of departure from equilibrium at any given observation temperature To. Therefore if a given polymeric material of fixed chemical composition can be manipulated (see below) at the molecular level to give a series of specimens with significantly different Tg values, it becomes possible to conduct a set of experiments at a single temperature To but at significantly different values of undercooling (Tg - To). For the case of gas sorption experiments this is a particularly useful idea since the measurements are carried out with the gas always at the measurement temperature To but with the absorbing substrate (glassy polymer) at a variable effective temperature (to be defined below). We therefore have the possibility of separating the effect of temperature of the substrate from that of the gas in the temperature dependence of the sorption process, something not achievable when both the gas and the substrate are heated or cooled together.

3.1.1 Enthalpy - Temperature Relationships

Figure 3-1 is a schematic of the enthalpy - temperature profile for two glassy polymers of the same chemical composition, P1 and P2, but with different glass transition temperatures Tg1 and Tg2 ($Tg1 < Tg2$). Both materials follow the same liquid temperature - enthalpy equilibrium line above the glass transition temperatures where $\partial \underline{H}/\partial T = Cp_L$. As P2 becomes a glass upon cooling below Tg2, the temperature - enthalpy behavior departs from the equilibrium line and follows the nonequilibrium glassy line described by $\partial \underline{H}/\partial T = Cp_g$. P2 would follow the equilibrium line below Tg2 if the cooling rate was sufficiently slow, but these rates are not experimentally accessible; an amount of excess enthalpy is frozen into the glassy material.

P1 becomes a glass at Tg1, at which point it also deviates from the equilibrium liquid curve and follows the glassy curve given by $\partial H/\partial T = Cp_g$. At a given temperature To below Tg1, P1 and P2 are in two different enthalpy states. The excess enthalpy in P1 is equal to $(Cp_L-Cp_g)(Tg1-To)$, and the excess enthalpy in P2 is equal to $(Cp_L-Cp_g)(Tg2-To)$. At To, the difference between the enthalpy of P1 and P2 is equal to $(Tg1-Tg2)(Cp_L-Cp_g)$ (a negative quantity). A sorption experiment conducted at a temperature To below Tg1 would therefore compare the solubility of a gas at a given temperature in a material of common chemical structure (i.e. polystyrene) but in different enthalpy states. It is the purpose of this paper to correlate this difference in enthalpy states with measured differences in the solubilities in the two glassy polymers.

Since both enthalpy and volume are known to be influenced similarly by sub-Tg annealing of glassy polymers, there is reason to believe that a correlation of excess volume, instead of enthalpy, with gas solubility could be equally well constructed. We prefer to use the frozen-in enthalpy because by definition (H = U + PV) it accounts for the volumetric state of the material and its internal energy. The latter reflects the molecular motions of the material into which gas is sorbing. While large scale thermal motion of chain molecules is frozen for glassy polymers, it is reasonable to expect that some short range motions persist and that these motions are diminished as T drops farther below Tg. To the extent that these short range thermal agitations reduce the equilibrium amount of gas which can be sorbed into a glassy substrate at sorption equilibrium, a correlation based on H, rather than V, should be superior. If thermal motions in all the substrates are identical or if they have no influence on the gas solubility at sorption equilibrium, then volume or enthalpy correlations can be used equally well to explain the gas sorption behavior in glassy polymers.

3.1.2 Development of T*

An adjusted temperature scale will be useful to compare the solubilities of samples with different Tg's so that the comparisons are made at equal polymer enthalpy states. We define a temperature T* as the temperature which a glass must assume in order to reach the enthalpy equal to that at the equilibrium state at To, the temperature of measurement Above Tg, T* is equal to the measurement temperature since the liquid or rubber is in an equilibrium state. Below Tg, T* is equal to the temperature necessary to reduce the enthalpy by an amount equal to the excess enthalpy defined above. T* is defined as :

$$T^* = To - [(Tg - To)(Cp_L-Cp_g)]/Cp_g \qquad (1)$$

Thus for a given value of To, the value of T* depends on the Tg and the difference in heat capacities between the glassy and rubbery states. Figure 3-1 shows schematically the calculation of T* at a given temperature To for P1 and P2. P2 has a higher Tg than P1 and therefore contains more excess enthalpy at To. A greater reduction in temperature (lower T*) is necessary for P2 to attain the equilibrium enthalpy associated with temperature To. Thus P2 is considered to exist at a lower effective temperature; it is "colder" than P1 in the solubility measurements at To.

The gas solubility is expected to be higher in P2 than in P1 at temperatures below Tg2 since P2 has a lower effective temperature T* [It is commonly observed that S increases as measurement temperature decreases; generally this trend has been attributed [16] to the increased condensibility of the gas rather than the state of the material into which the gas is sorbing.] At a fixed temperature, measuring the gas solubility in a series of glasses with increasing Tg's is equivalent to lowering the temperature of the polymer thereby explaining the observed result of increasing solubility with increasing Tg.

The temperature scale T* can also be used to analyze the temperature dependence of the gas solubility in a glass compared to the behavior in the corresponding rubber. The temperature dependence of the gas solubility in a polymer sample above its Tg would follow the temperature of the measurement since T* = To above Tg. In the glassy state, the temperature of the measurement changes directly with To while the state of enthalpy of the polymer changes with T*. Since

$$T^* = To(1 + ((Cp_L - Cp_g)/Cp_g)) - Tg(Cp_L - Cp_g)/Cp_g, \qquad (2)$$

$$\partial T^* = \partial To(1 + ((Cp_L - Cp_g)/Cp_g)) \qquad (3)$$

Thus T* changes more rapidly than To. Plotted against To, the temperature dependence of S in the glassy state should be stronger (more exothermic) than in the rubbery state.

These thermodynamic arguments regarding solubility and its temperature dependence were used to analyze the measured solubility behavior of CO_2, CH_4, and Ar in a model set of polystyrene samples with different Tg's.

3.2 Experimental Section

Two polystyrene (PS) homopolymers were obtained from Polysciences, Inc. with nominal molecular weights of 250,000 (PS4) and 20,000 (PS1). Two additional PS samples were prepared by fractionating PS1. Methanol was slowly dripped into a 10% PS1 / toluene solution until a significant amount of polymer had precipitated. This filtered precipitate (PS2) was fractionated again to yield PS3. All four polystyrene samples were annealed in vacuum just below Tg for 4 days to remove residual solvent.

3.3 Results and Discussion

3.3.1 Polystyrene Fractionation

Table 3-1 summarizes the DSC and GPC results for the four PS samples. The glass transition temperature (Tg) for polystyrene varied from 52 °C to 107 °C as Mn varied from 2,100 to 200,000 g/mole. None of the measured Tg values was influenced by the presence of any sorbed gases at the pressures and temperatures used in this study. The NMR spectra of the four samples were all identical and indistinguishable from polystyrene spectra in the literature, precluding the existence of

externally added plasticizers or other significant impurities. The GPC chromatograms for PS1, PS2 and PS3 are shown in Figure 3-2. Low molecular weight oligomers of styrene appear in large concentration in PS1 (Figure 3-2). Evidently the presence of these oligomers is responsible for the depression of the Tg of PS1 to 52 °C. The fractionation steps used to prepare PS2 and PS3 successively removed the low molecular weight oligomers and increased the proportion of the longer chains. Removal of the oligomers increases Tg of PS2 to 72 °C and the Tg of PS3 to 90 °C. The GPC results for PS4 indicated a broad distribution of long chains with no low molecular weight species.

3.3.2 Solubility Coefficient

The behavior of the solubility coefficients (measured at 1 atm) for CO_2, Ar and CH_4 as a function of temperature for PS1 and PS4 is shown in figures 3-3a - 3-3c. The heats of solution (Es, Kj/mole) obtained from these plots for PS1 (Tg = 52 °C) were -12.4, -4.6, and -6.2 for CO_2, CH_4, and Ar, respectively; the heats of solution (Kj/mole) for PS4 (Tg = 107 °C) were larger in magnitude at -22.0, -15.7 and -11.3, respectively. The observed order of increasing gas solubilities ($Ar < CH_4 < CO_2$) reflects the trend of increasing gas boiling temperatures and increasing Lennard - Jones gas potentials. This is consistent with reported correlations of increasing gas solubility with increasing ease of gas condensibility [17].

For all three gases examined, the heats of solution for the polystyrene with the higher Tg (PS4) were more exothermic than the heats of solution for the polystyrene with the lower Tg (PS1). This behavior can be understood by considering the enthalpy of PS1 and PS4 at the measurement temperatures. Over the temperature range 20 - 90 °C, PS1 was primarily in the melt (liquid state) and the glass transition zone, while PS4 was in the glassy state. The enthalpy of PS1 was therefore either equal to or close to the equilibrium state enthalpy, while PS4 always contained an amount of excess enthalpy. Comparing the gas solubilities on a temperature scale based on the measurement temperature To instead of T* predicts a stronger temperature dependence (more exothermic) for the solubility in a glass than in the corresponding rubber, which is what was observed.

The CO_2 solubility in PS at 30 °C decreased as the Tg of the PS sample decreased (see Figure 3-4). This dependence of the solubility on Tg was less pronounced at higher test temperatures, and disappeared when all the materials became rubbery (see Figures 3-3a-3-3c). Again, the solubility behavior is consistent with the different enthalpy states that the PS samples assume at 30 °C. At 30 °C PS4 has the largest excess enthalpy since it has the highest Tg, and PS1 has the smallest amount of excess enthalpy. Using the adjusted temperature scale T* to compare the polymer gas solubilities on an equal enthalpy basis, PS4 reaches a lower temperature T* than PS1 in order to attain the enthalpy equal to the equilibrium enthalpy at 30 °C. Since CO_2 solubility increases as the temperature decreases, the polymer at the lower temperature T* (PS4) should have a higher solubility, as observed. Assuming the differences in solubilities among polymer samples depends

on the amount of excess enthalpy, all observed differences in gas solubilities should disappear as the highest Tg of the samples is approached. This is observed in figures 3-3a - 3-3c.

The effect of excess enthalpy on the gas solubility and the heat of solution can be quantified using equation 3 with an estimate of the value of $(Cp_L-Cp_g)/Cp_g$. For polystyrene, a value of 0.6 was chosen based on [18]. According to our proposal outlined above, solubilities of gases in polystyrene with equal states of enthalpy should be identical. This comparison is possible by plotting the gas solubilities in PS as a function of T*. Figures 3-5a - 3-5c display the CO_2, Ar and CH_4 solubility coefficients for PS1 and PS4 as a function of 1/T*. The heats of solution (Kj/mole) for CO_2, CH_4 and Ar in PS calculated from figures 7 through 9 lie in the range -12.1 to -9.1, -7.0 to -3.5 and -6.3 to -4.7, respectively. The range of Es is larger for CH_4 and Ar due to the increased uncertainty in the measurement.

Table 3-2 summarizes the heats of solution for CO_2, CH_4 and Ar in PS1 and PS4 calculated from solubilities plotted against the measurement temperature (Es) and against the adjusted temperature scale T* (E*). The E* values in table 3-2 are the midpoint of the range of values calculated from each of figures 3-5a - 3-5c. The values for E* are close to those of Es for PS1 since PS1 is in the rubbery state and the early glass transition region over the temperature range explored. The use of equal enthalpy states to compare solubilities in glasses instead of the measurement temperature results in convergence of the solubility and heat of solution values for PS samples with different glass transition temperatures. This convergence is most clearly seen for the CO_2 data.

IV. Gas Transport in Polybutadiene Treated with Aqueous Bromine

Diffusion, solubility and permeability coefficients were measured for He, CO_2, Ar and CH_4 in polybutadiene (PB) and in polybutadiene reacted in the solid state to various extents with aqueous bromine. Analysis of the sorption curves and x-ray emission spectra showed that the bromination created a heterogeneous membrane with an outer brominated skin and an unreacted core. The gas diffusion and permeability coefficients decreased for CO_2, Ar and CH_4 and remained unchanged for He with bromination.

4.1 Experimental Section

The polybutadiene homopolymer (PB) used in this study was obtained from Polysciences, Inc. and has a molecular weight of 200,000 g/mole with 90% 1,4 addition. Films (about 0.2 mm thick) were made by static casting a 5% toluene solution onto a flat Teflon surface. The cast films were lightly crosslinked with a 5 Mrad dose of electron beam radiation before removal from the casting surface.

The conditions used to brominate the PB films have already been described in detail elsewhere [19]. The films were submerged in a 0.1 M aqueous bromine solution at room temperature for various reaction times. After the reaction, the films were rinsed in distilled water for 24 hours and placed in a vacuum oven at room temperature until there was no weight loss.

As the bromination reaction proceeded, the PB films became orange and increased in weight and size. At complete reaction, the final weight uptake, W_∞, of a polybutadiene specimen was a factor of three greater than the original weight, W_o; this amount of weight gain corresponds to the incorporation of two bromine atoms for each double bond in the polybutadiene [20,21]. The extent of reaction will hereafter be referred to as a fraction of the maximum achievable weight increase, i.e. $W(t)/W_\infty$ or $W(t)/(3\ W_o)$. The glass transition temperature (Tg), determined by differential scanning calorimetry, increased as the bromination reaction proceeded. The Tg increased from -80°C for the unreacted PB to 35 °C for a film reacted to 2.7 % extent of reaction.

4.2 Results

4.2.1 Permeability Coefficients

The gas permeability coefficients for He, CO_2, CH_4 and Ar at 35 °C were measured for the untreated PB and the bromine modified PB films in a variable volume permeability apparatus [22]. The permeability coefficients are shown in Figure 4-1 as a function of percent of reaction. The permeability coefficients for CH_4, Ar and CO_2 decreased dramatically as the bromination reaction proceeded; with extent of bromination of only 0.5% the permeabilities of CO_2, CH_4 and Ar dropped by over an order of magnitude and at 2.7% extent of reaction the CO_2 permeability coefficient dropped by almost three orders of magnitude and those for Ar and CH_4 were too low to measure in the present apparatus. The permeability coefficient of He, however, remained relatively unaffected up to 2.7 % bromination.

The changes in permeability with bromination were accompanied by changes in the gas selectivity. The selectivity characteristics can be evaluated by comparing the ratio of the permeability coefficients for a gas pair (ideal separation factor, μ) in the reacted and unreacted films. The values of μ for the gas pairs He/CH_4, He/CO_2 and CO_2/CH_4 increased from 0.74, 0.16 and 4.5, respectively, in the original PB to 14, 1.7 and 8.3, respectively, in the 0.5 % brominated film. For He/CO_2, μ further increased to 56 in the film reacted to 2.7 %. Brominating PB creates a membrane which greatly increases the ideal separation factor for separations involving He; furthermore, the brominated PB is a good barrier material for relatively large gas molecules such as CH_4 and Ar.

4.2.2 Solubility Coefficients

The permeability coefficient of a penetrant in a homogeneous material can be broken down into a product of the diffusion (D) and solubility (S) coefficients [23]. It is of interest to determine whether the large decrease in P with bromination was caused by decreases in D or S. The D and S

coefficients for CO_2, Ar and CH_4 were measured at 35 °C in a pressure decay sorption apparatus to explore the source of the permeability decrease. The details of the experimental apparatus and analysis technique are described elsewhere [17].

The equilibrium solubility of CO_2 at 35 °C as a function of extent of bromination is shown in Figure 4-2. Up to 14.3 % bromination the CO_2 solubility decreased by 35% of its original value. Ar and CH_4 displayed similar decreases in solubility with bromination. Although there are measurable decreases in the gas solubility coefficients with reaction, these are insufficient to account for the orders of magnitude decreases in the permeability coefficient.

4.2.3 Diffusion Coefficients

The diffusion coefficients for CO_2, Ar and CH_4 at 35 °C were determined from the half-times of the sorption curves [17]. The results for CO_2 are shown in Figure 4-3. The diffusion coefficients decreased monotonically with increasing bromination. For 2.7 % reacted films, the diffusion coefficients for Ar, CO_2 and CH_4 decreased by two orders of magnitude from their original values. By 14.3 % extent of reaction, the diffusion coefficient for CO_2 had decreased by over three orders of magnitude.

4.3 Discussion

The large decreases in the permeability coefficient are attributable primarily to changes in the diffusion coefficient. However, assuming the bromine reacted uniformly throughout the PB film to give a homogeneous material, the measured decreases in the diffusion and solubility coefficients do not sufficiently account for the decreases in the permeability coefficient. At 2.7 % bromination, the permeability coefficient for CO_2 decreased by a factor of 690 while the combined change in the diffusion and solubility coefficients account for a decrease of only a factor of 90 in permeability (assuming $P = DS$).

Insight to this apparent inconsistency is obtained by considering the shapes of the sorption curve. The sorption curve for CO_2 in the film reacted to 2.7 % is shown in Figure 4-4; it has a sigmoidal shape with a slow initial gas uptake rate. This curve is indicative of a composite material with an outside skin layer of much lower diffusion coefficient than the bulk material [13]. For this type of composite, the gas permeability coefficient will not be a simple product of the half-time diffusion coefficient and solubility coefficient. This complication occurs in composite membranes because the diffusion coefficient calculated from the half time of the sorption curve is not equal to the steady state effective diffusion coefficient. Evidently, the bromine did not react homogeneously throughout the material, and therefore agreement between the observed changes in the permeability coefficient and the product of the solubility and diffusion coefficients should not be expected.

Direct evidence for the formation of a skin layer during the bromination reaction was obtained using SEM. A film brominated to 14.3 % extent was frozen in liquid nitrogen and fractured. Specimens for SEM were prepared from the fractured sample by mounting at two different

orientations and gold coating. Figure 4-5a shows an example of the roughened surface texture (observed to various extents for all the brominated materials) when viewed normal to the film surfaces. Figure 4-5b shows a SEM micrograph of the fractured edge viewed almost parallel to the film surface; this micrograph clearly reveals an outer skin layer which is brighter than the inner core. The image in this micrograph was formed using the secondary electron detector with an accelerating voltage of 25 kV. The contrast seen can be identified with differences in the atomic number of the species in the material. Species with higher atomic numbers (Br atom vs C atom) yield a higher concentration of backscattered electrons and appear brighter [24]. Since the skin layer is brighter than the core, it clearly contains a higher bromine concentration.

The energy dispersive x-ray analyzer in the SEM was used to quantitatively characterize the brominated skin layer [25]. The relative bromine concentration as a function of distance from the film edge was determined from the x-ray emission spectrum (xes) and is displayed in Figure 4-6. Using the data from Figure 4-6, it is straightforward to estimate that bromination to 14.3 % yields a membrane with an outer shell which is completely brominated (100 % reacted) and which has a thickness of approximately 15 % of the bulk thickness.

The CO_2 diffusion coefficient in this fully brominated PB skin can be estimated once the thickness is known. This calculation involves simulating the experimental sorption curve using a finite difference method for modeling gas uptake in a composite [13]. In the simulation, gas first diffuses through the outer skin then into the central core. There is no net flux through the membrane in a sorption experiment since the penetrant gas enters from all sides. The composite was assumed to consist of a skin layer (the 100 % brominated PB comprising 15% of the total thickness) with a low diffusion coefficient and a central core of pure PB. Although bromine was detected to a small extent into the core region, this was ignored to simplify the simulation.

The diffusion coefficients from the simulated and the measured sorption curves were calculated from the half times. The diffusion coefficient of the pure PB core was fixed based on the measured value of 5.0×10^{-6} cm^2/sec determined in our laboratory while the diffusion coefficient in the brominated skin was adjusted to create a match between the measured and simulated D. The CO_2 diffusion coefficient in the brominated PB skin was determined from the simulation to be 1.0×10^{-9} cm^2/sec with an error of 30% assuming an error of 25% in determining the skin thickness. Thus, the solid state bromination of PB to full conversion decreases the diffusion coefficient by 3.5 orders of magnitude.

We suggest that the decrease in gas diffusion with bromination in PB is brought about by three factors. First of all, the removal of unsaturation in PB could decrease the diffusion coefficient by decreasing the ease of hole formation for a diffusional jump in the polymer; evidence for this effect was seen by the decrease in the diffusion coefficient of octadecane in PB by a factor of two upon hydrogenation [26]. Secondly, the addition of bulky Br decreases the diffusion coefficient by

decreasing the chain flexibility, similar to the decrease of the N_2 diffusion coefficient in PB by a factor of 10 upon methyl substitution to yield poly(2,3-dimethyl butadiene) [27]. Finally, the addition of the polar Br side group increases the chain cohesive energy, decreasing the diffusion coefficient; halogen-substituted polycarbonates have lower gas diffusion coefficients than methyl-substituted polycarbonates [28]. Thus, the structural changes in brominated PB responsible for the lowering of the gas diffusion coefficient include both decreasing the chain flexibility and increasing the chain cohesive energy.

The CO_2 permeability coefficient for brominated PB can be estimated from the skin layer thickness data. As indicated by the xes analysis of the 14.3 % brominated sample, the skin thickness (as a percent of the total thickness) is equal to the extent of bromination. The skinned brominated PB is a composite laminate arranged in series with respect to the direction of gas transport, and the permeability coefficient for such a laminate can be expressed as:

$$1/Ppar = v_1/P_1 + v_2/P_2$$

where Ppar is the composite permeability coefficient, P_1 is the permeability in the skin layer with volume fraction v_1 and P_2 is the permeability of the bulk material with volume fraction v_2. For the 2.7 % brominated film, P_1 (the skin layer permeability) was calculated to be 0.021 barrer assuming that P_2 was pure PB and Ppar was the measured value of 0.75 barrer.

Given the estimated permeability and diffusion coefficients for CO_2 in the brominated skin layer, the solubility coefficient of the skin can be estimated assuming the P in the homogeneous skin layer can be expressed as a product of *D* and *S*. *Using this relation, the solubility coefficient for* CO_2 in the fully brominated PB was estimated as .0021 cc(STP)/cc/cm Hg, a factor of 5 lower than the CO_2 solubility in unmodified PB.

V. Gas Transport in Solvent Crazed Microporous Membranes

A microporous membrane was produced from the controlled solvent crazing of a block copolymer with cylindrical microphase separation. The crazing procedure involved a solvent which selectively swelled the cylindrical microdomains. Osmotic pressure was the driving force to expand the cylindrical regions while the stressed glassy matrix provided an upper limit on the size of the voids created. Gas transport properties of the material were monitored as a function of solvent treatment.

5.1 Experimental Section

The technique of sequential anionic polymerization was used to synthesize a diblock copolymer of polystyrene -b- polymethyl methacrylate (PSPMMA) with a composition of 31% PMMA (determined by proton NMR) and a PS Mw of 150,000. Microtomed thin samples from static cast (*THF solvent) films displayed a morphology of* PMMA cylinders with a diameter of 250 Å in a

continuous matrix of PS. The PMMA domains in a static cast PSPMMA film were selectively swollen by immersion into a mixture [29] of 10% water and 90% isopropanol at 70 °C for various treatment times.

5.2 Results and Discussion

5.2.1 Morphological Changes with Solvent Treatment

Untreated PSPMMA films were transparent and brittle and became milky white and flexible upon solvent treatment. Figures 5.1 and 5.2 display the increase in PSPMMA weight and thickness with solvent exposure time. The weight of the film increased with exposure time until it leveled off at 170% increase. Similarly, the volume of the film increased with exposure time, and this increase in volume was equal to the volume of the absorbed solvent. The solvent was completely desorbed from the film after exposure to vacuum at room temperature for 24 hours. The thickness remained in the expanded state after the solvent was removed and collapsed to the original value upon annealing for 4 hours at 100 °C.

Dramatic morphological changes were observed in SEM of the surface (Figure 5.3) and edge (Figure 5.4) views of a film solvent treated to a weight increase of 170%. The edge view was taken from a sample frozen in liquid N_2 then cracked. These micrographs display the uniform spherical character of the voids incorporated during the solvent treatment and were visually estimated to be 500 Å - 1000 Å in diameter. This pore diameter was also characterized using bubble point analysis with isopropanol as the wetting fluid. The bubble point analysis was run by Dr. Ramesh Hegde of Millipore Corp., Bedford, MA. *The results report a pore diameter of between 200 and 500 Å ± 10%.* Thus, the pore size of the limiting constrictions probed by the bubble point fluid is smaller than the pore size observed in the SEM. Dr. Hegde also measured the N_2 BET isotherm of a fully treated PSPMMA film and determined the surface area to be 41.2 m^2 / g. This is significantly larger than the surface area of the pores seen in the SEM of 11.2 m^2 / g , suggesting there are voids in the films smaller than those visible in the SEM which are accessible by N_2 in the BET measurement.

The process of solvent uptake in PSPMMA involves a sharp advancing front (see Figure 5.5) separating swollen from unswollen polymer. This front completely penetrates the film after a solvent treatment of about 40% weight increase. It is thought that the solvent treatment before the front penetrates the film results primarily in the formation of new pores, while the solvent treatment after the front has penetrated the film results primarily in the growth and coalescence of these existing pores.

5.2.2 Gas Transport Changes with Solvent Treatment

The measured diffusion coefficients (see Figure 5.6) for CO_2, CH_4 and Ar in PSPMMA at 30 °C increased with solvent treatment. D for Ar and CH_4 were not measurable over the complete solvent treatment range due to limited solubility. It is believed that this measured diffusion coefficient corresponds to the gas diffusion through a polymer matrix and not to diffusion through a

micropore (Knudsen diffusion) since the D increases equally for all of the gases with solvent treatment. The ratio of gas diffusion coefficients would have changed from the original values associated with polymer diffusion if Knudsen diffusion was being measured. Although pore and polymer diffusion probably occur simultaneously in the final solvent crazed material, the pore diffusion rates are not accessible using the present apparatus.

There is a dramatic increase in the diffusion coefficients between the solvent treatment times of 560 minutes and 980 minutes. This interval brackets the time (approximately 600 minutes) the advancing swollen front reaches the center of the film. If the pores created before 600 minutes of solvent treatment are isolated, the observed minimal increase in gas diffusion coefficient is expected. Once there are conductive paths between the pores, however, there should be a dramatic increase in the diffusion coefficient. Conductive paths among the pores should occur once the pores begin to grow in size and impinge on each other. Significant growth and coalescence among the pores is thought to commence soon after the advancing front fully penetrates the film. Thus, the increase in diffusion coefficient is reasonable based on the position of the swollen front and assuming the pores which are formed initially are isolated.

The permeability coefficients as a function of solvent treatment for He, Ar, CH_4 and CO_2 are shown in Figure 5.7. There is a large increase in the permeability for all gases at a treatment level of 18% weight increase, and by 75% weight increase the permeability coefficients increased from the untreated values by five orders of magnitude. Table 5.1 shows the ideal separation factors for He / Ar and CO2 / Ar as a function of solvent treatment as well as those predicted assuming gas transport by Knudsen diffusion. Based on these selectivity results, the mechanism governing gas transport seems to change from permeation through a polymer matrix to flow through a pore at a solvent treatment of 18% weight increase.

A dramatic increase in the permeability coefficient, based on the results of the diffusion coefficient, was expected after a solvent treatment of 40% weight increase. The permeability, however, increased at 18% weight increase, suggesting there are conductive paths to gas transport which percolate through the film in advance of the swollen front. The diffusion coefficient is more representative of the average morphological features, and would not indicate the presence of a small concentration of conductive paths which are capable of registering large changes in the permeability coefficient.

VI. Summary

This work has addressed several issues of gas transport control in heterogeneous polymer systems. An SB block copolymer with well ordered lamellar microstructure facilitated the simulation of transient CO_2 , Ar and CH_4 sorption experiments using the pure component homopolymer behavior as input. Comparison of measured and model-calculated block copolymer

diffusion coefficients revealed significant differences in gas transport through the polybutadiene regions of the block copolymer and the corresponding polybutadiene homopolymer. The polybutadiene of the block copolymer contained an additional temperature dependent resistance to gas transport (permeability or diffusion) not observed in the polybutadiene homopolymer, and this resistance displayed a selectivity to gases based on size. Restriction of chain motion caused by the chemical connection of the polybutadiene to the glassy polystyrene in the heterogeneous SB block copolymer underlies this observed extra resistance to gas transport. The equilibrium solubility of the CO_2 in the B regions of the SB diblock was not influenced by these restrictions on molecular motions; equilibrium solubilities of CO_2 in SB at various temperatures were adequately described by a volume-fraction weighted combination of the homopolymer solubilities.

The dependence of the gas solubility in polymers on the chemical nature of the gas and polymer and on the state of enthalpy of the polymer was explored using polystyrene. A comparison of the solubility coefficients based on equal polymer enthalpy states instead of the measurement temperatures explained the trends observed in a series of polystyrenes of varying Tg's. The most notable trend is the large increase (by as much as a factor of 1.9) in S (measured at 30 °C) with *increasing* substrate Tg.

Two experimental techniques to control gas transport in heterogeneous polymers were pursued. Bromination of polybutadiene created a film with a skin layer of brominated PB and a virtually unreacted core. The skin layer dramatically reduced the permeation to Ar, CO_2 and CH_4, while decreasing only slightly the permeation to He. The *bromination reaction* produces a material which selectively permeates gases based on size with the cutoff size larger then He and smaller the Ar. A microporous membrane was produced through the controlled solvent cracking of a diblock copolymer. A high degree of control over the pore size and distribution is possible using the solvent crazing technique because the microporous morphology is dependent on the small size and tight distribution of the starting block copolymer morphology. As the porous structure penetrated the film, the gas permeation and diffusion dramatically increased and the transport mechanism changed from diffusion through a polymer matrix to flow through a pore.

VII. References

1. Takada, K.; Matsuya, H.; Masuda, T.; Higashimura, T. *J. App. Polym. Sci.* **1985**, *30*, 1605.

2. McBride, J. S.; Massaro, T. A.; Cooper, S. L. *J. Appl. Polym. Sci.* **1979**, *23*, 201.

3. Chiang, K. T.; Sefton, M. V. *J. Polym. Sci., Polym. Phys. Ed.* **1977**, *15*, 1927.

4. Odani, H.; Taira, K.; Nemoto, N.; Kurata, M. *Bull. Inst. Chem. Res., KyotoUniv.* **1975**, *53*(2), 216.

5. Odani, H.; Taira, K.; Nemoto, N.; Kurata, M. *Polym. Eng. Sci.* **1977**, *17* (8), 527.

6. Odani, H.; Uchikura, M.; Taira, K.; Kurata, M. *J. Macromol. Sci., Phys.* **1980**, *B17* (2), 337.

7. Csernica, J.; Baddour, R. F.; Cohen, R. E. *Macromolecules*, **1987**, *20*, 2468.

8. Csernica, J. PhD. Thesis, Massachusetts Institute of Technology, August, 1989.

9. *Diffusion in Polymers*; Crank, J.; Park, G. S., Eds.; Academic Press Inc.: New York, 1968.

10. Crank, J. The Mathematics of Diffusion, 2nd ed.; Claredon: Oxford, 1975.

11. Petropoulos, J. H. *J. Polym. Sci., Polym. Phys. Ed.*, **1985**, *23*, 1309.

12. Rogers, C. E. in Polymer Permeability, Comyn, J., Ed., Elsevier: London, 1985.

13. Csernica, J.; Baddour, R. F.; Cohen, R. E. *Macromolecules*, **1989**, *22*, 1493.

14. Kita, H.; Murakaoka, M.; Tanaka, K.; Okamoto, K. *Polym. J.*, **1988**, *20*(6), 485.

15. Michaels, A. S.; Parker, R. B., Jr. *J. Polym. Sci.* **1959**, *41*, 53.

16. Stannett, V. T.; Koros, W. J.; Paul, D. R.; Lonsdale, H. K.; Baker, R. W., " Recent Advances in Membrane Science and Technology " in *Advances in Polymer Science*, 32, Springer - Verlag New York, 69, 1979.

17. Rein, D. R.; Csernica, J.; Baddour, R. F.; Cohen, R. E. *Macromolecules*, **1990**, *23*, 4456.

18. Maeda, Y.; Paul, D. R. *J. Polym. Sci. Polym. Phys. Ed.*, **1987**,

25, 957.

19. Csernica, J.; Rein, D. H.; Baddour, R. F.; Cohen, R. E. *Macromolecules* **1991**, *24*, 3612.

20. Canterino, P. J. In *Chemical Reactions of Polymers*; Fettes, E. M., Ed.; Interscience, New York, 1964.

21. Morrison, R. T.; Boyd, R. N. *Organic Chemistry*; Allyn and Bacon: Boston, MA, 1983.

22. ASTM D-1434, American Society for Testing and Materials, Philadelphia, PA, 1984.

23. Chern, R. T.; Koros, W. J.; Hopfenberg, H. B.; Stannett, V. T., in: D. R. LLoyd (Ed.), *Material Science of Synthetic Membranes*, ACS Symp. Ser. No. 269, American Chemical Society, Washington, DC, 1985.

24. Thomas, E. L. In Encyclopedia of Polymer Science and Technology; Mark, H. F.; Bikales, N. M.; Overberger, C. G. Menges, G.; Kroschwitz, J. I., Eds.; Wiley and Sons: New York, 1985; Vol. 4.

25. Price, F. P.; Gilmore, P. T.; Thomas, E. L.; Laurence, R. L. *J. Polym. Sci., Polym. Symp.* **1978**, *63*, 33.

26. Auerbach, I.; Miller, W. R.; Kuryla, W. C.; Gehman, S. D. *J. Polym. Sci.* **1958**, *28*, 129.

27. Van Amerongen, G. J. J. Polym. Sci. **1950**, *5*, 307.

28. Muruganandam, N.; Paul, D. R. *J. Membr. Sci.*, **1987**, *34*, 185.

29. Cowie, J. M.; Mohsin, M. A.; McEwen, I. J. *Polymer*, **1987**, *28*, 1569.

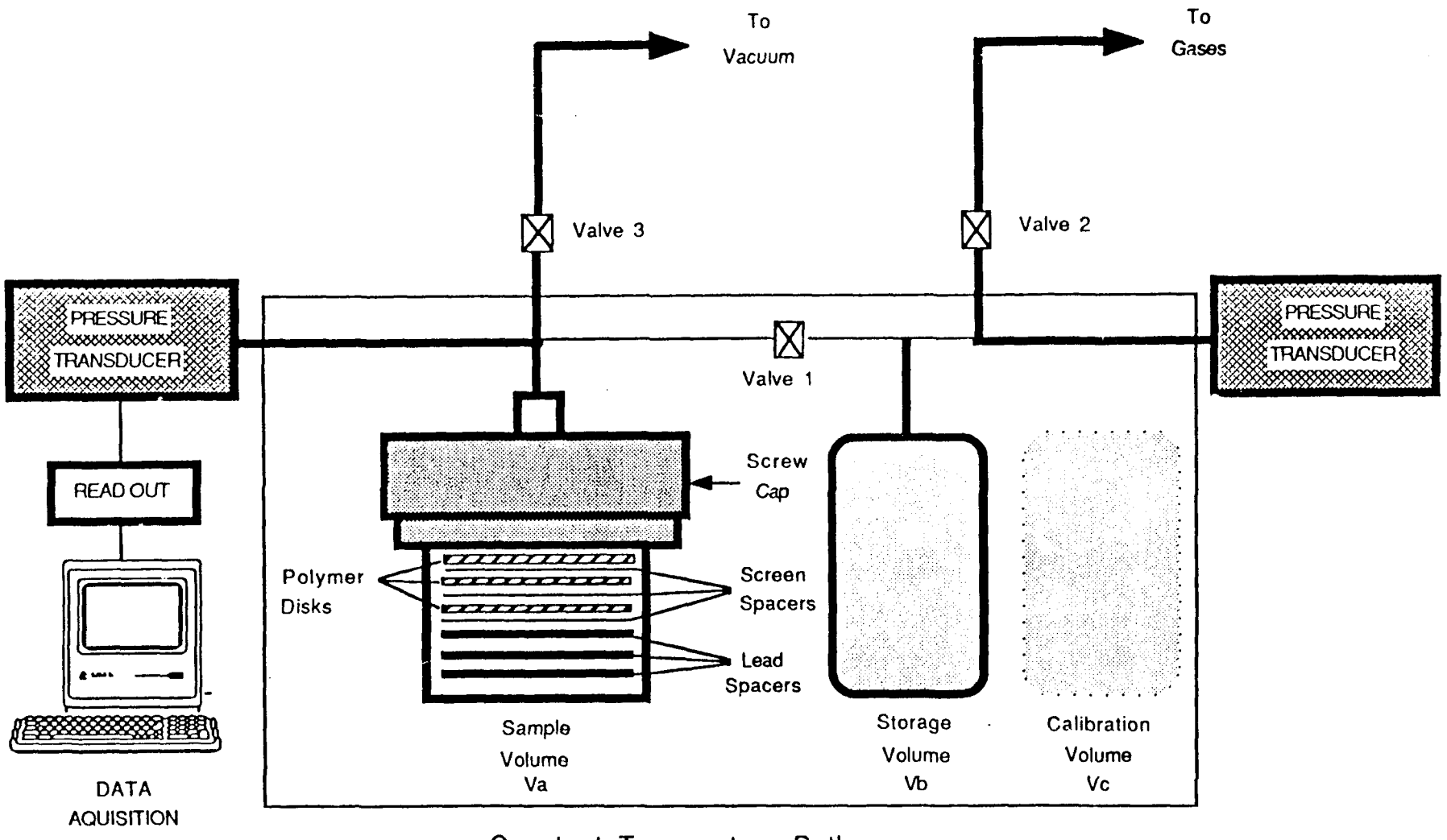

Figure 2-1. Schematic of dual-volume sorption apparatus

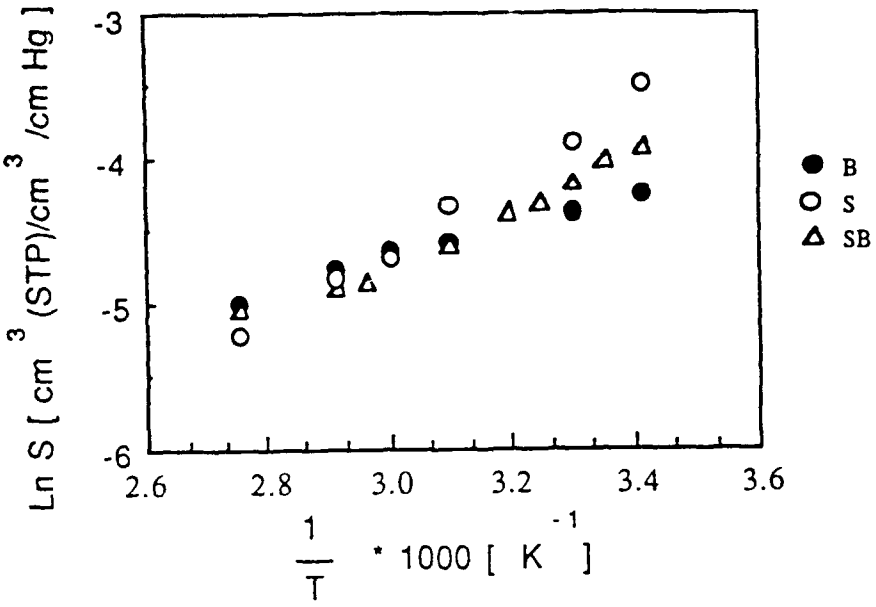

Figure 2-2. Temperature dependence of the equilibrium CO2 solubility coefficients for S, B, and SB

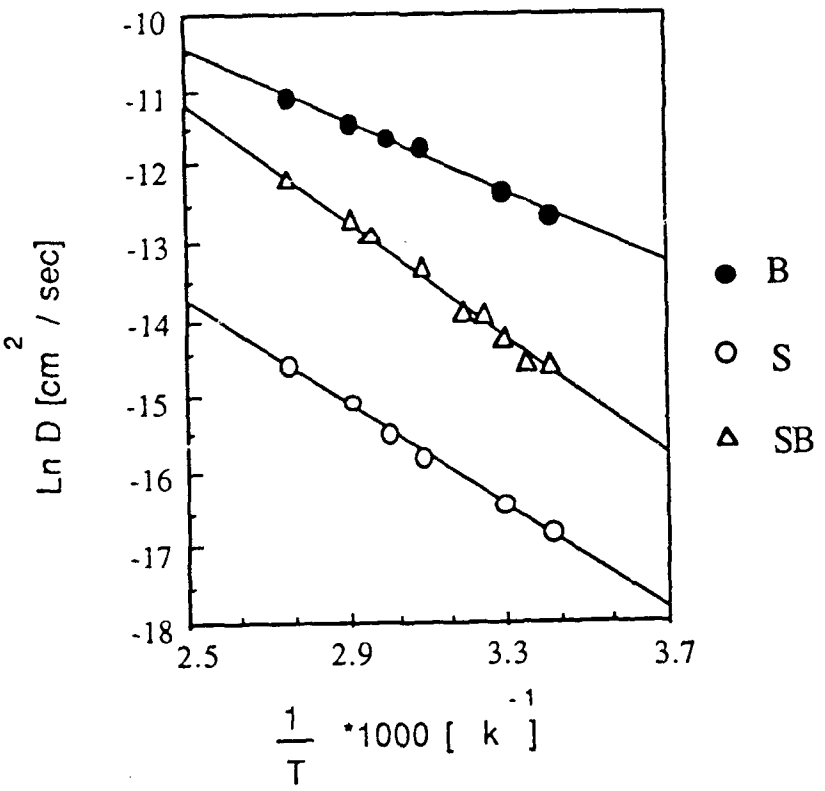

Figure 2-3a. Arrhenius plots of the diffusion coefficients for CO2 in S, B, and SB

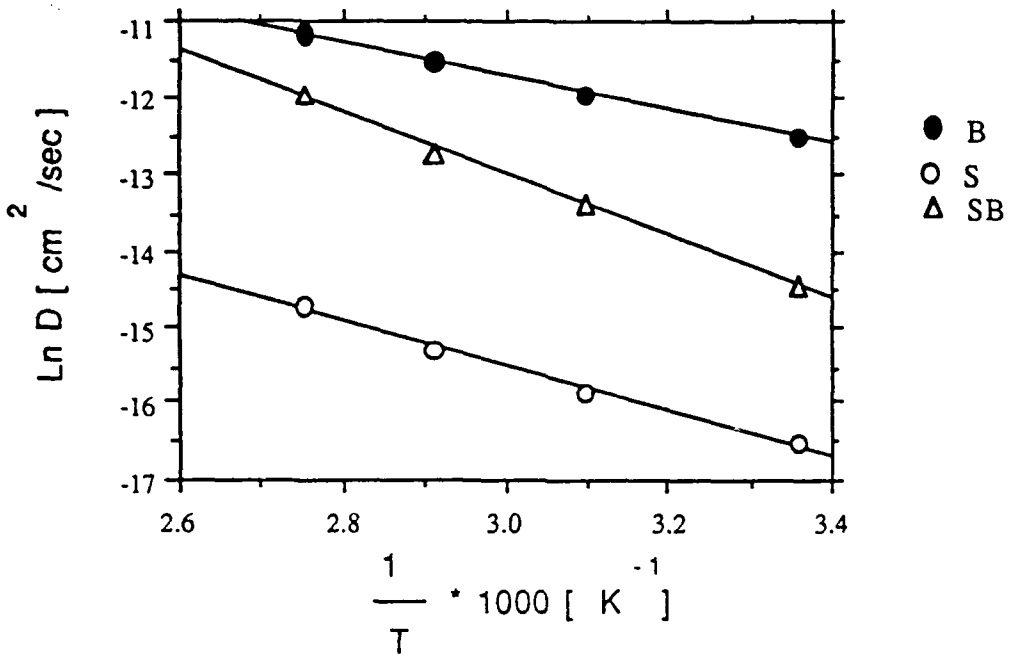

Figure 2-3b. Arrhenius plots of the diffusion coefficients for Ar in S, B, and SB

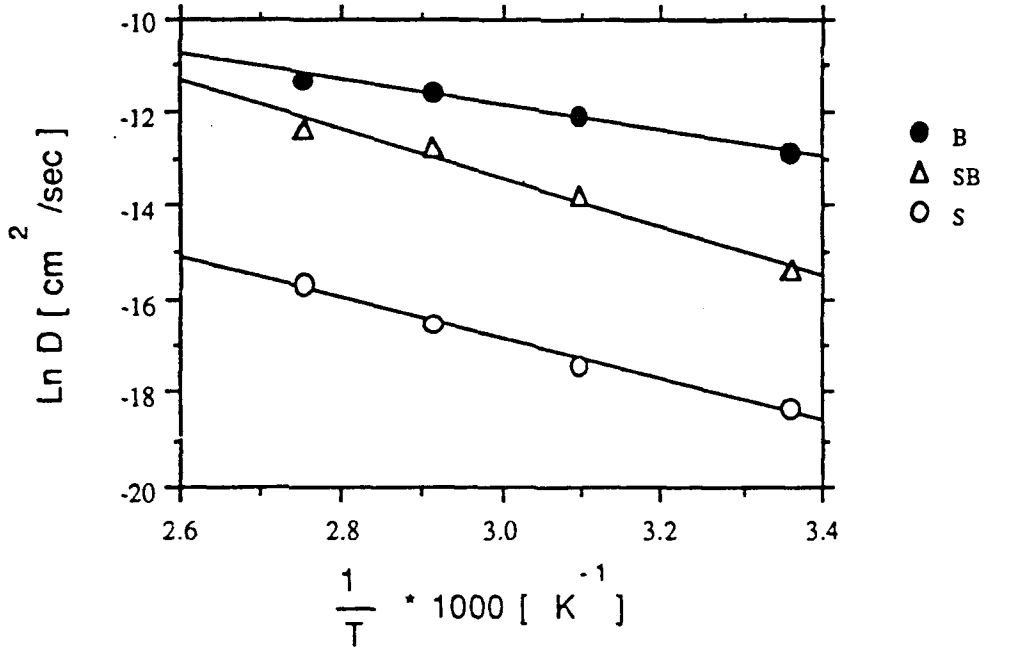

Figure 2-3c. Arrhenius plots of the diffusion coefficients for CH4 in S, B, and SB

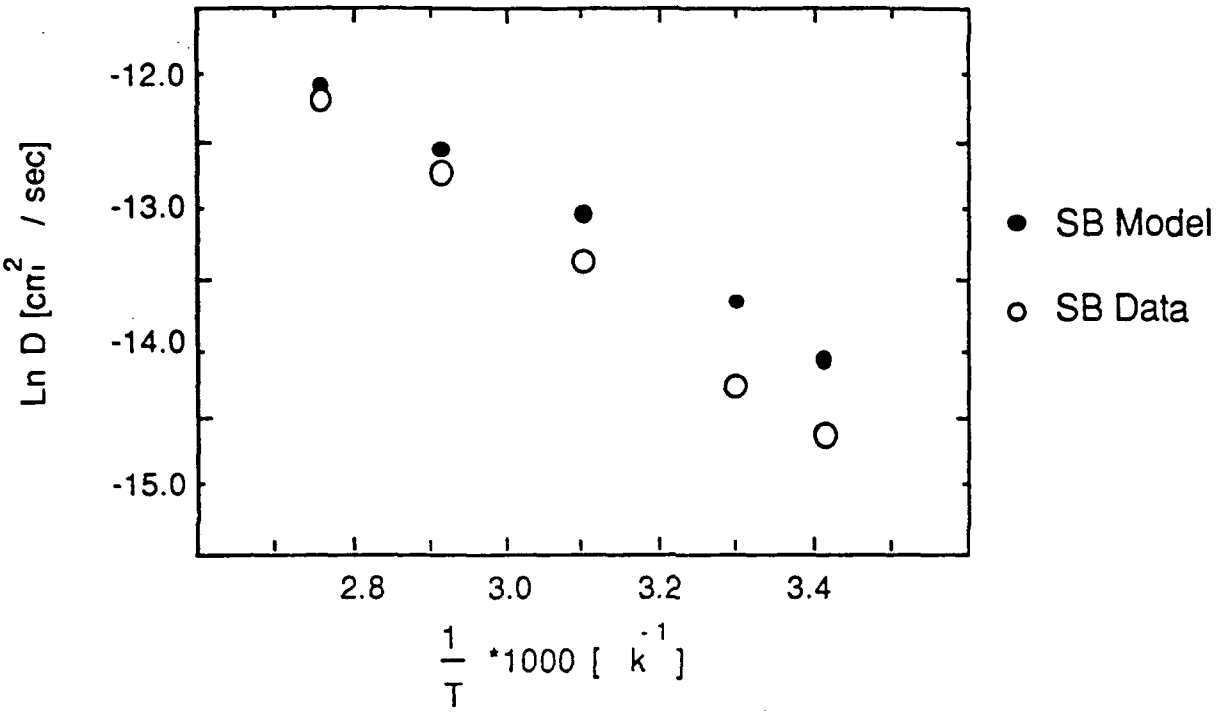

Figure 2-4a. Comparison of Arrhenius plots for measured and model generated CO2 diffusion coefficients

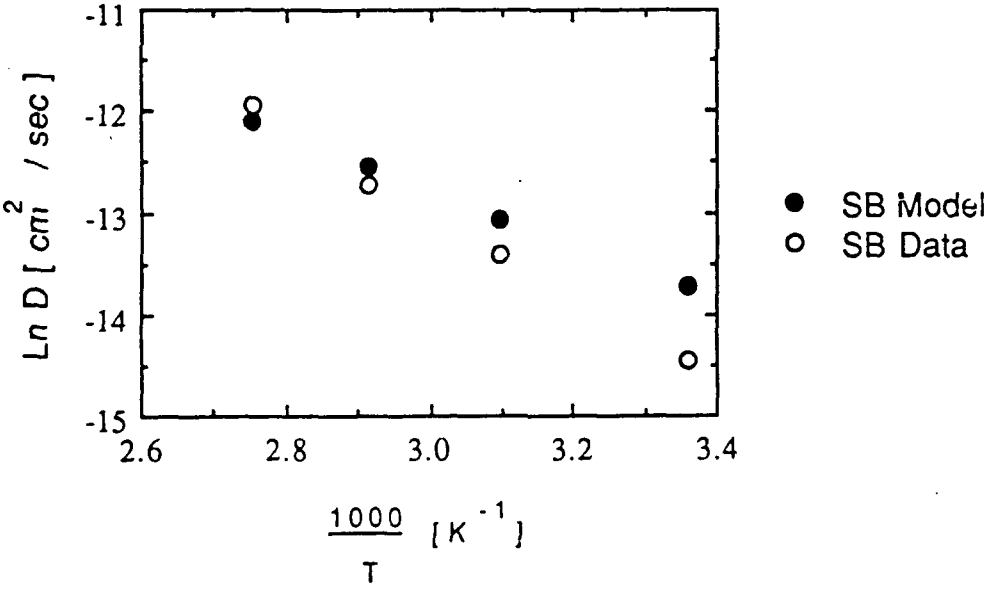

Figure 2-4b. Comparison or Arrhenius plots for measured and model generated Ar diffusion coefficients

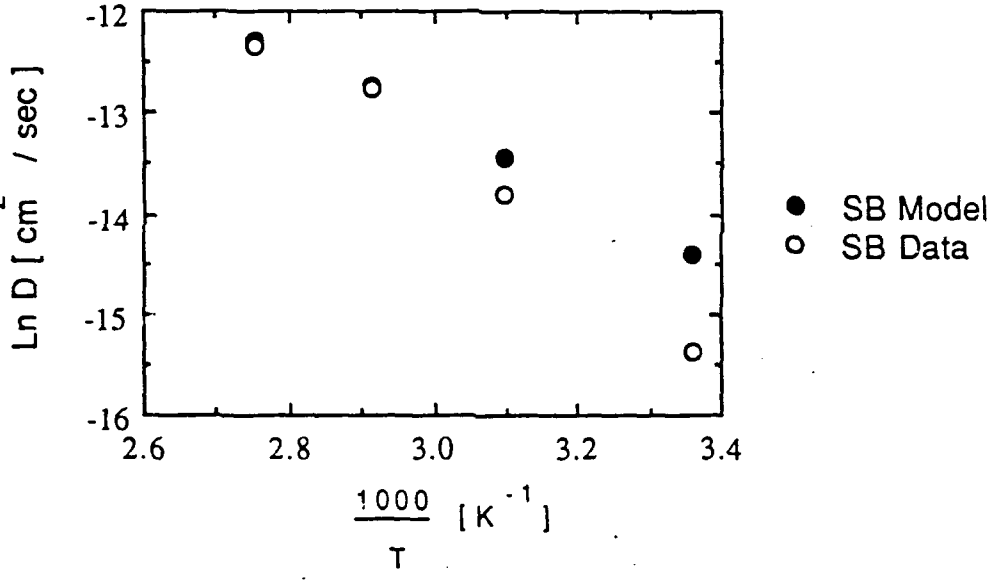

Figure 2-4c. Comparison of the Arrhenius plots for measured and model-generated CH4 diffusion coefficients

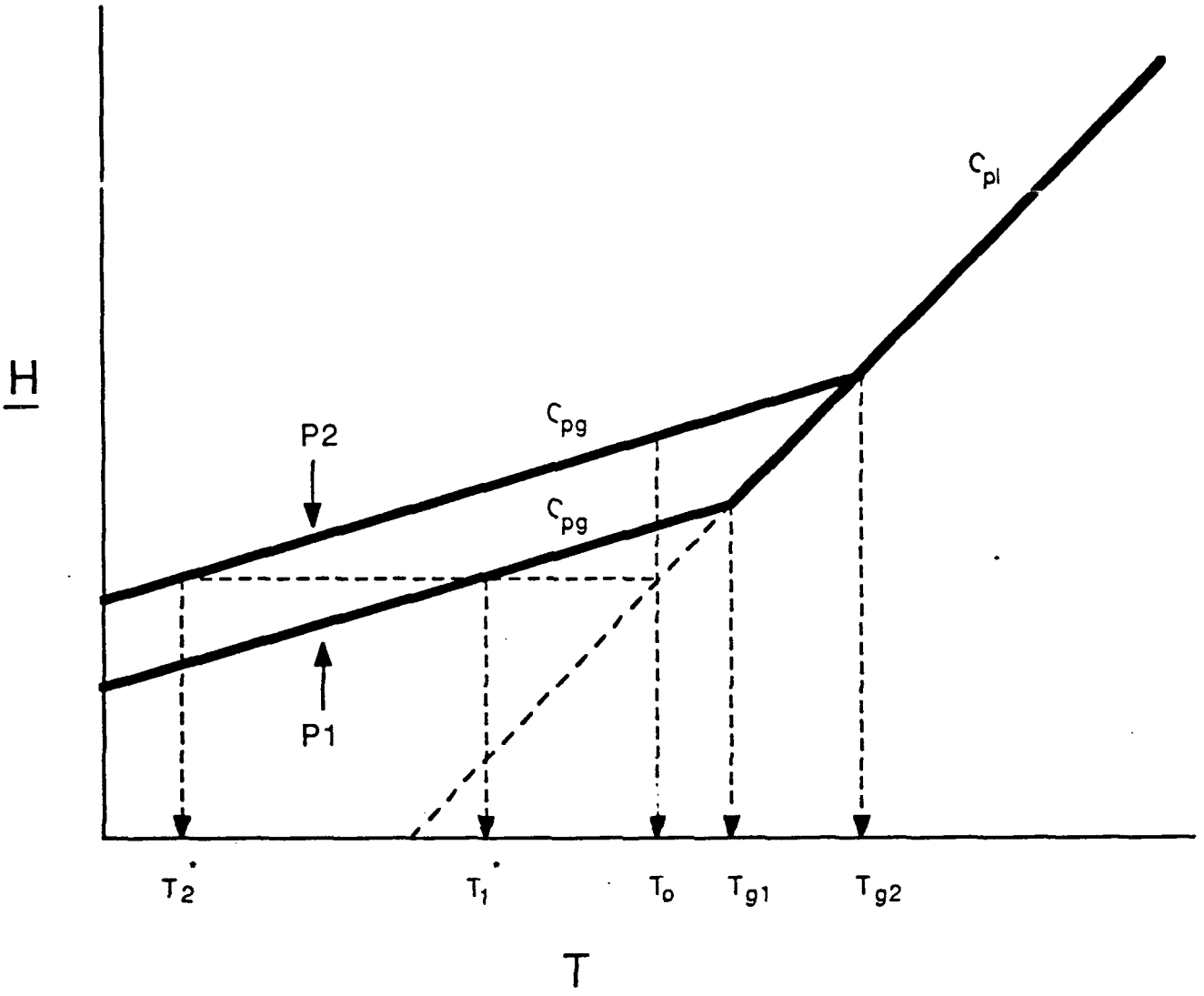

Figure 3-1. Temperature - enthalpy curve for polymers PS1 and PS2 with glass transition temperatures Tg1 and Tg2, respectively. T* is defined as the temperature which the polymer would have to assume to obtain the equilibrium value of enthalpy at temperature To.

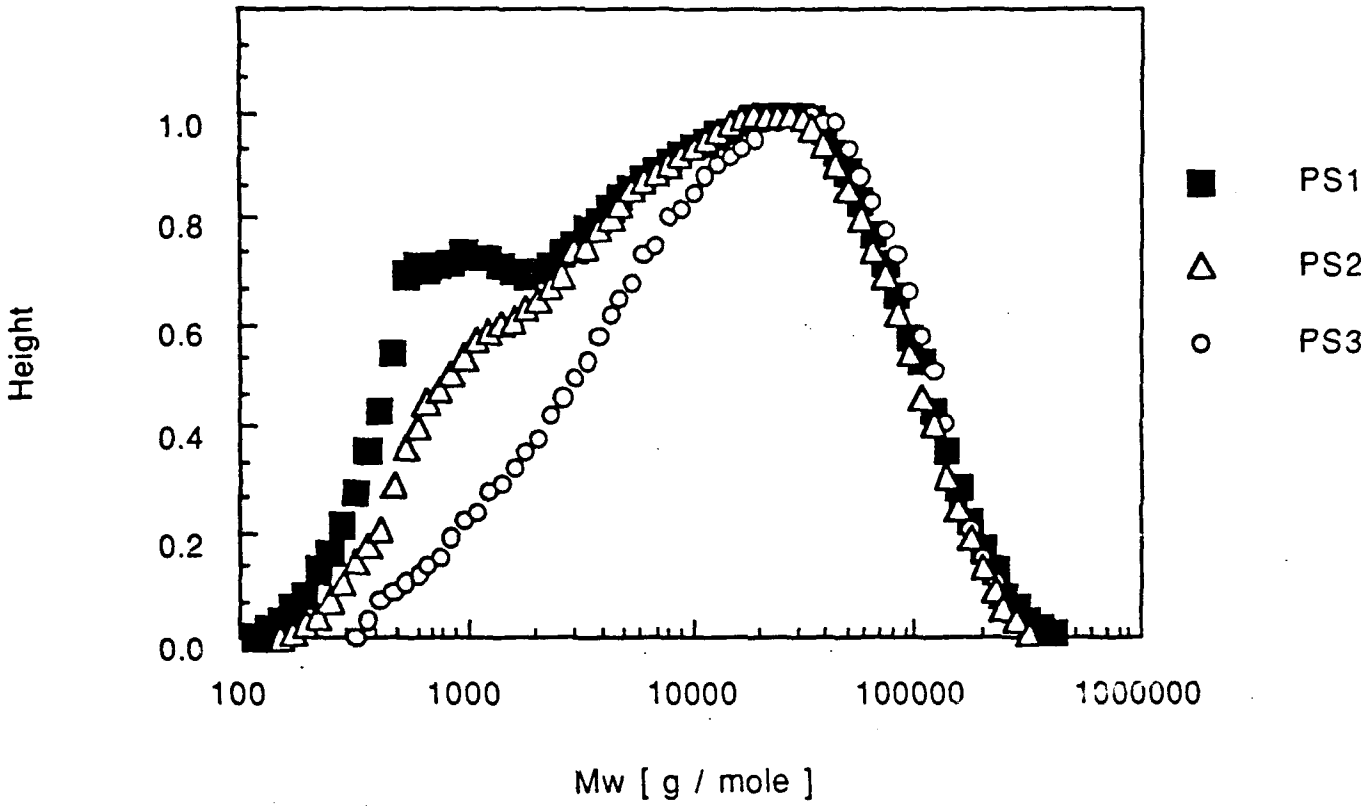

Figure 3-2. GPC chromatogram of PS1, PS2 (PS1 fractionated once), PS3 (PS1 fractionated twice).

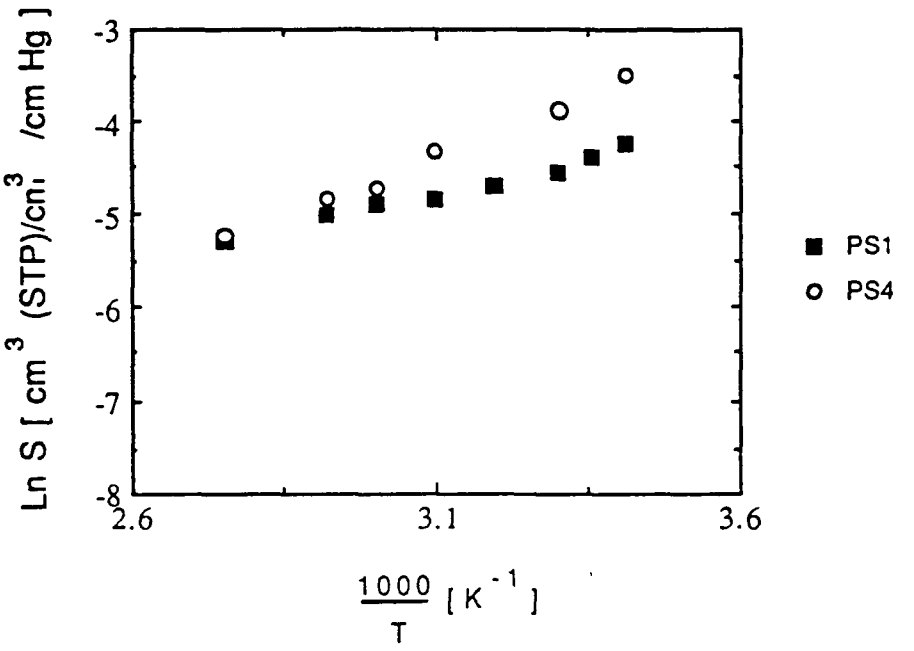

Figure 3-3a. Temperature dependence of the equilibrium CO2 solubility coefficients for PS1 and PS4.

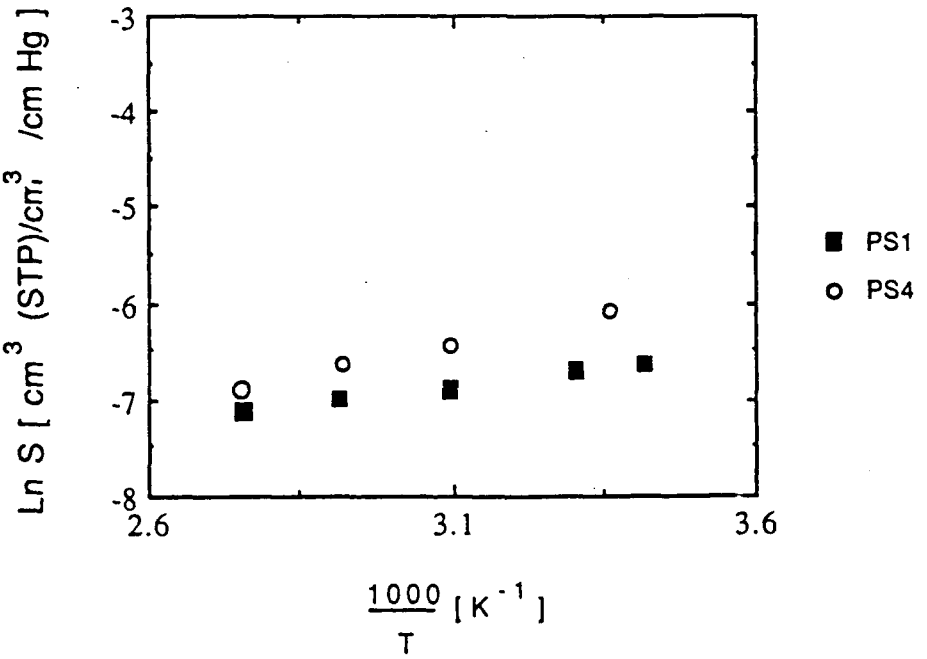

Figure 3-3b. Temperature dependence of the equilibrium Ar solubility coefficients for PS1 and PS4

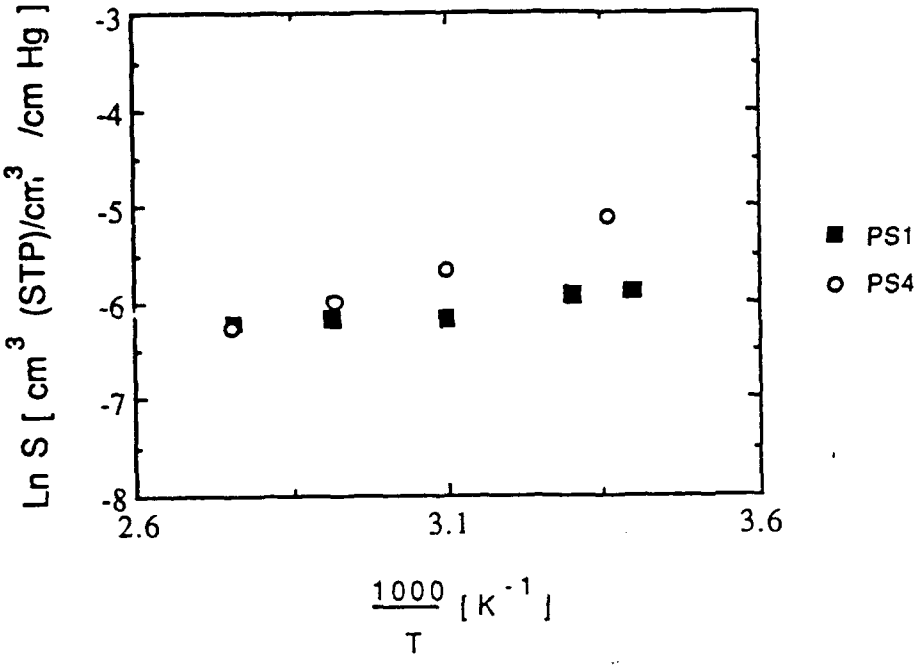

Figure 3-3c. Temperature dependence of equilibrium CH4 solubility coefficients for PS1 and PS4.

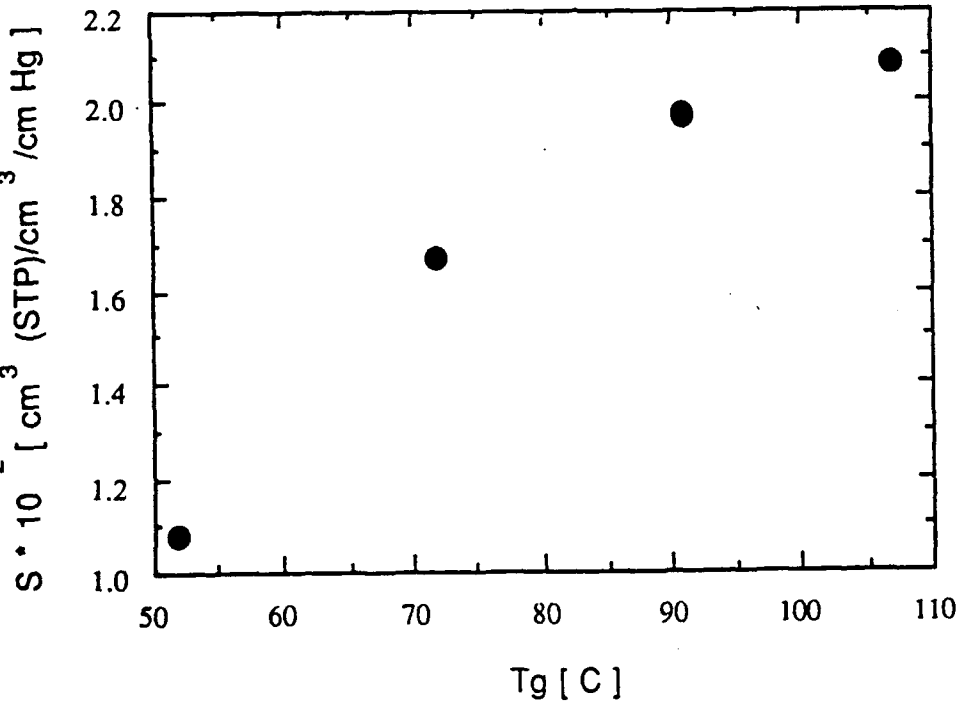

Figure 3-4. Effect of polystyrene Tg on the CO2 solubility at 30 °C

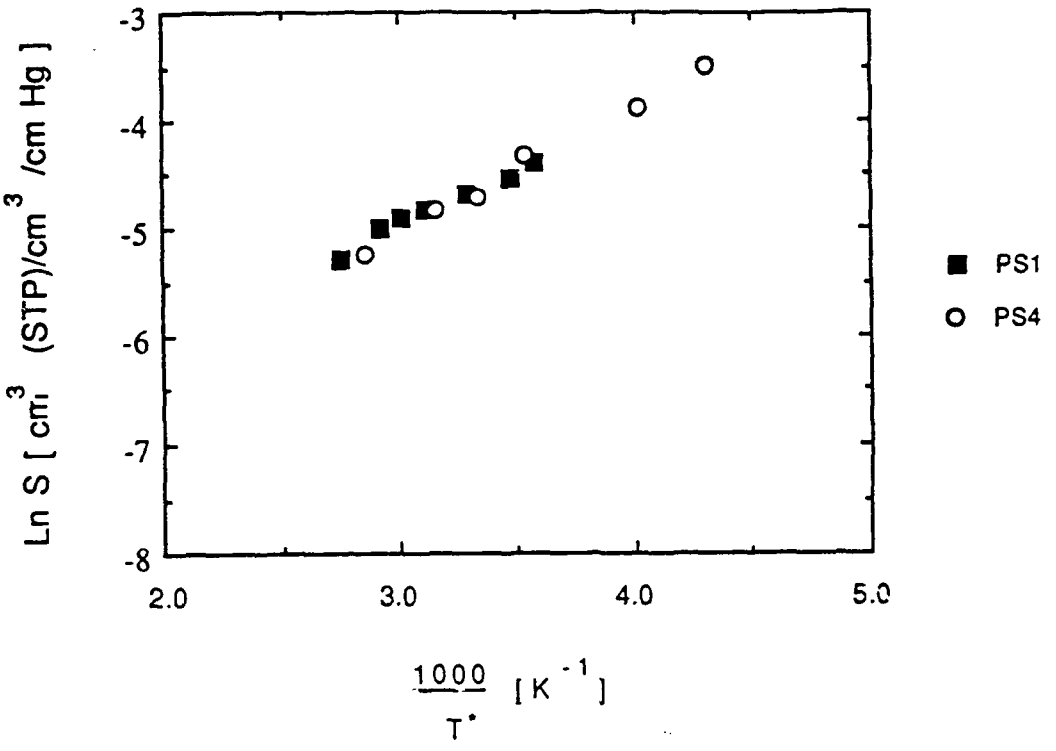

Figure 3-5a. Measured CO2 solubility in PS1 and PS4 compared at equal enthalpy states using the temperature scale T* and (CpL - Cpg)/Cpg = 0.6

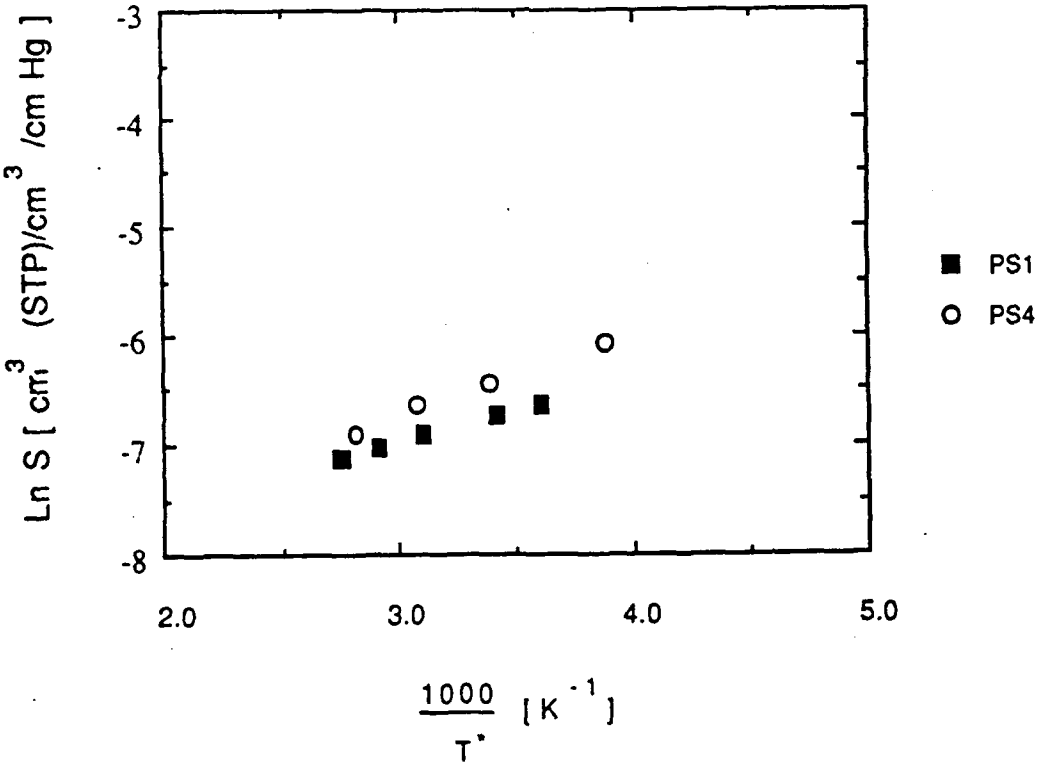

Figure 3-5b. Measured Ar solubility in PS1 and PS4 compared at equal enthalpy states using the temperature scale T* and (CpL - Cpg)/Cpg = 0.6

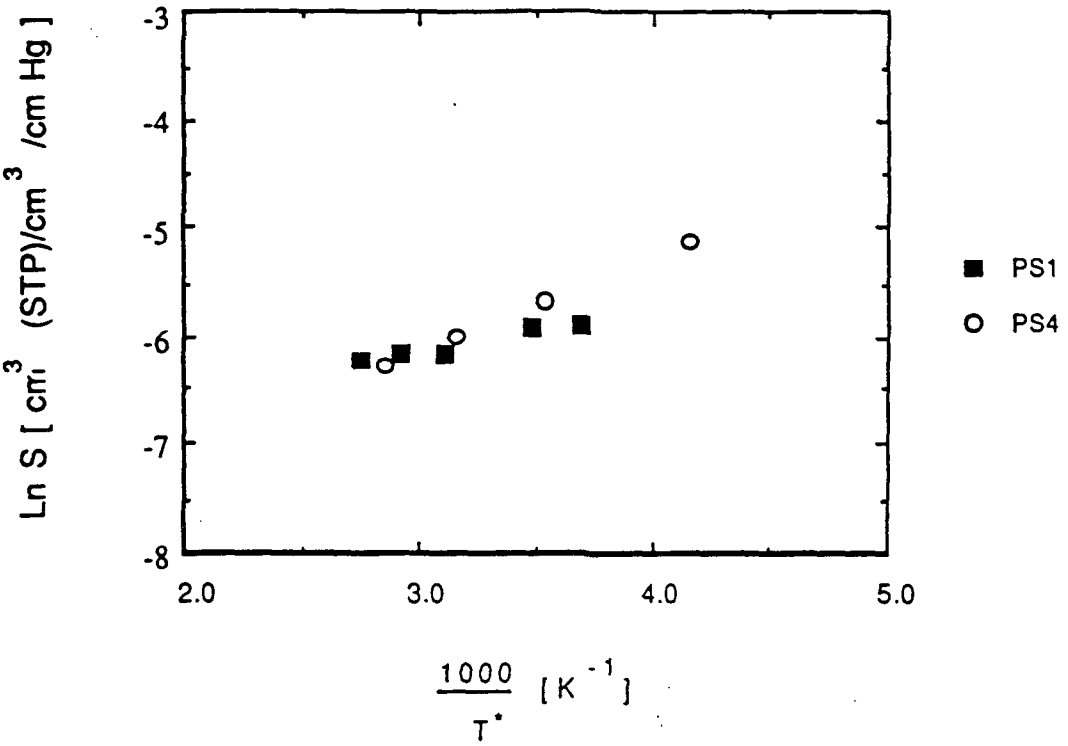

Figure 3-5c. Measured CH4 solubility in PS1 and PS4 compared at equal enthalpy states using the temperature scale T* and (CpL - Cpg)/Cpg = 0.6

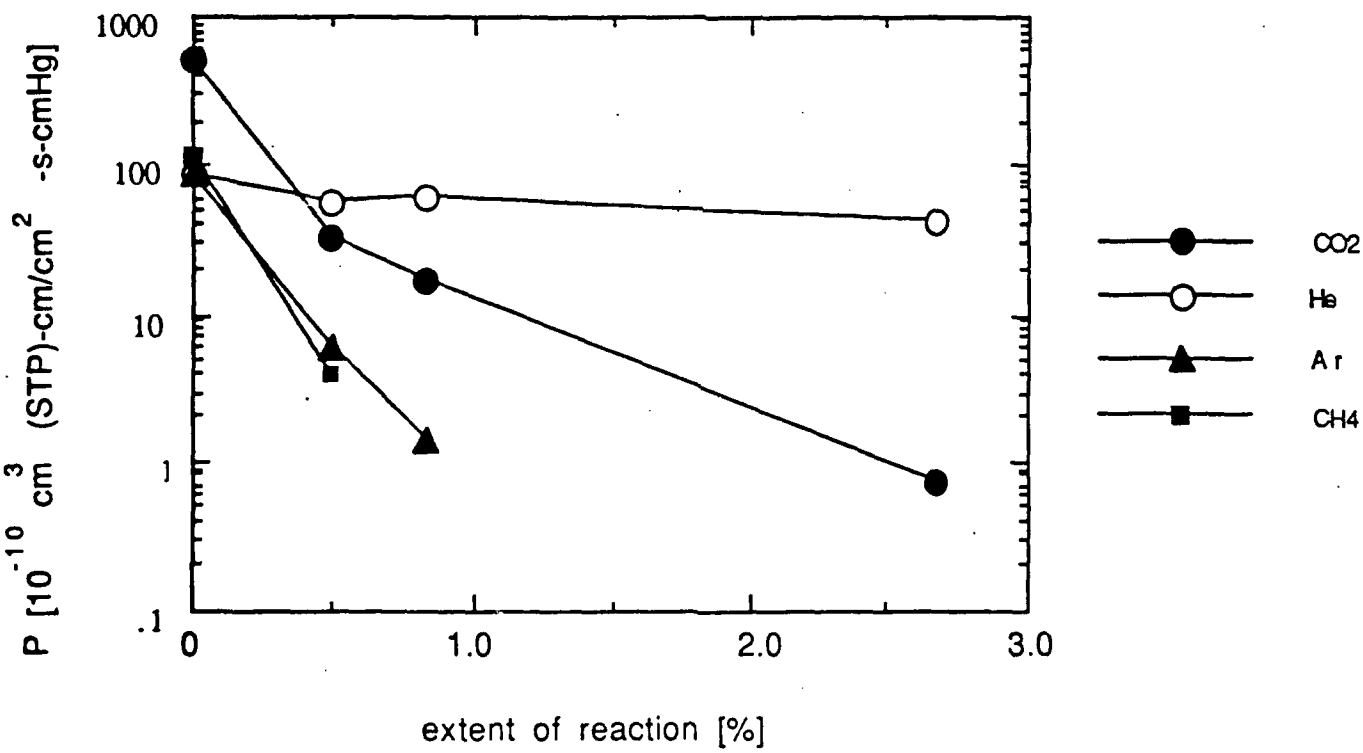

Figure 4-1. Permeability of gases at 35 °C in PB films reacted to various extents with complete reaction = 100 % in aqueous bromine

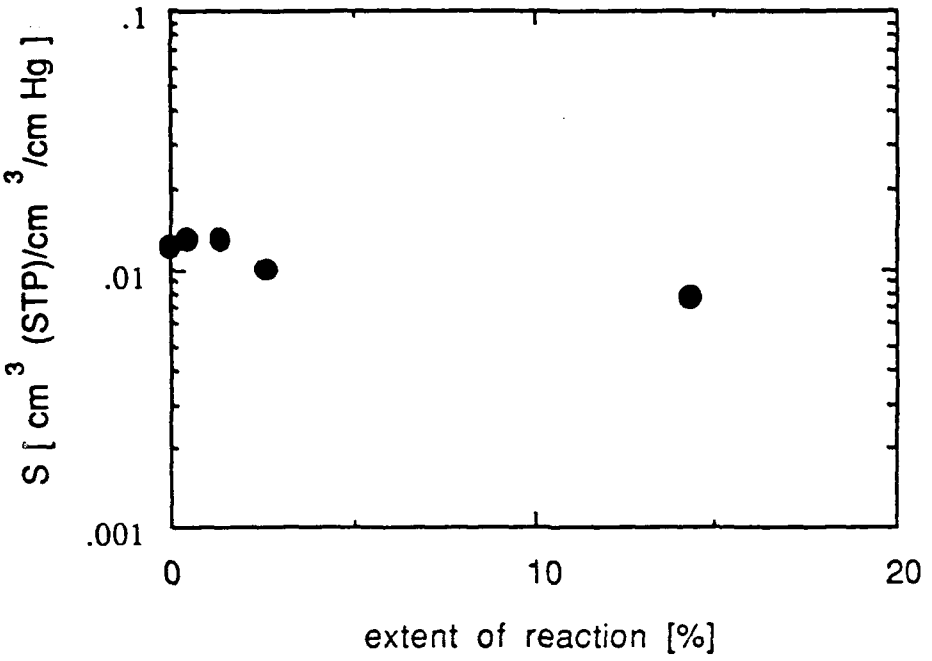

Figure 4-2. Solubility coefficient of CO2 at 35 °C in brominated PB films

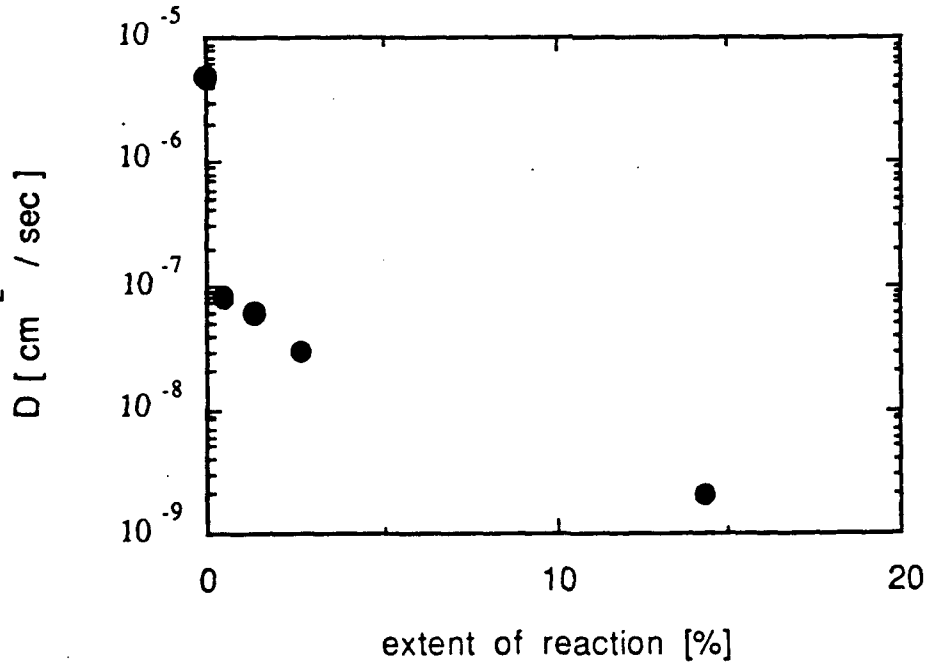

Figure 4-3. Diffusion coefficient of CO2 at 35 °C in brominated PB films

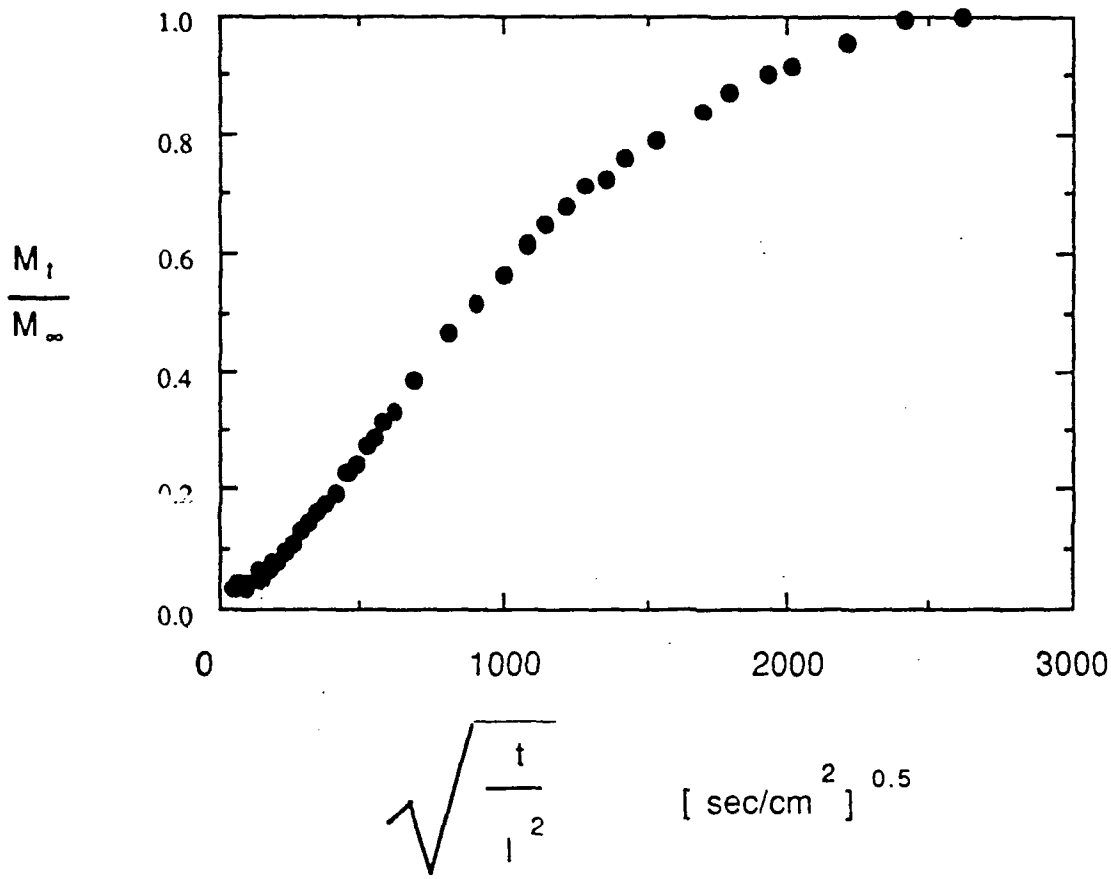

Figure 4-4. Sorption uptake curve for CO2 at 35 °C in a PB film brominated to 2.7% extent reaction. Sigmoidal shape indicates presence of skin layer.

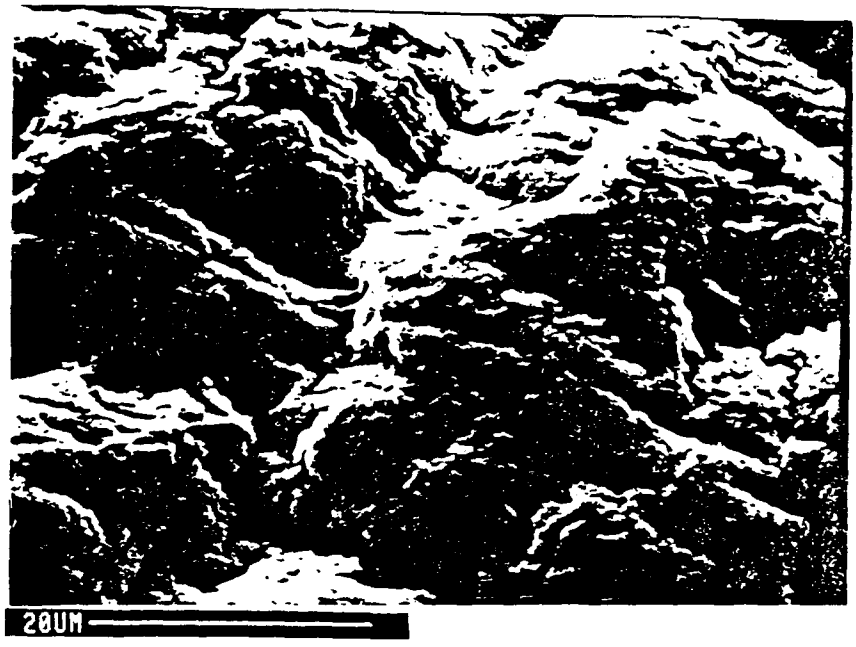

Figure 4-5a. SEM top view of PB film brominated to 14.3% extent of reaction

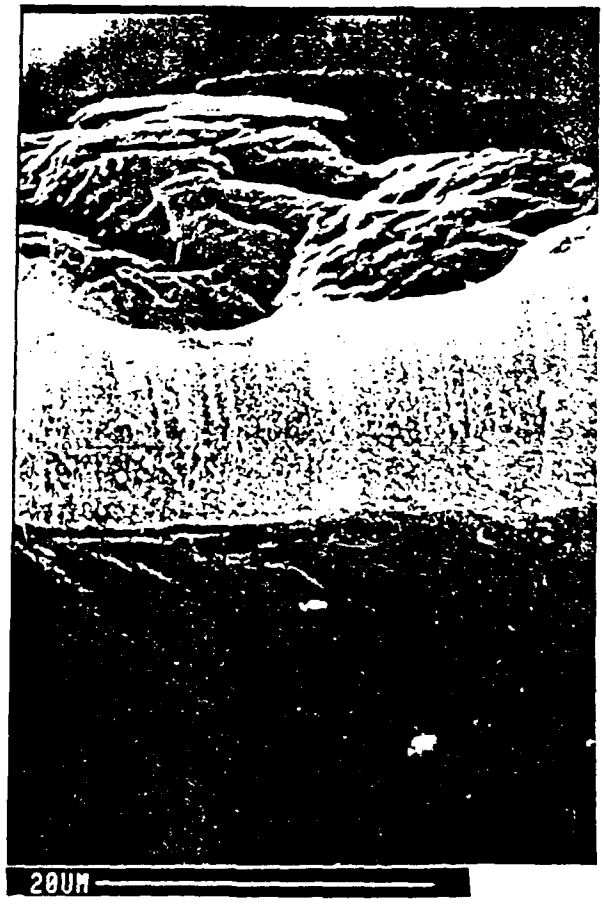

Figure 4-5b. SEM edge view of PB film brominated to 14.3% extent of reaction. Bright outside edge is brominated skin layer and total film thickness is 200 μ.

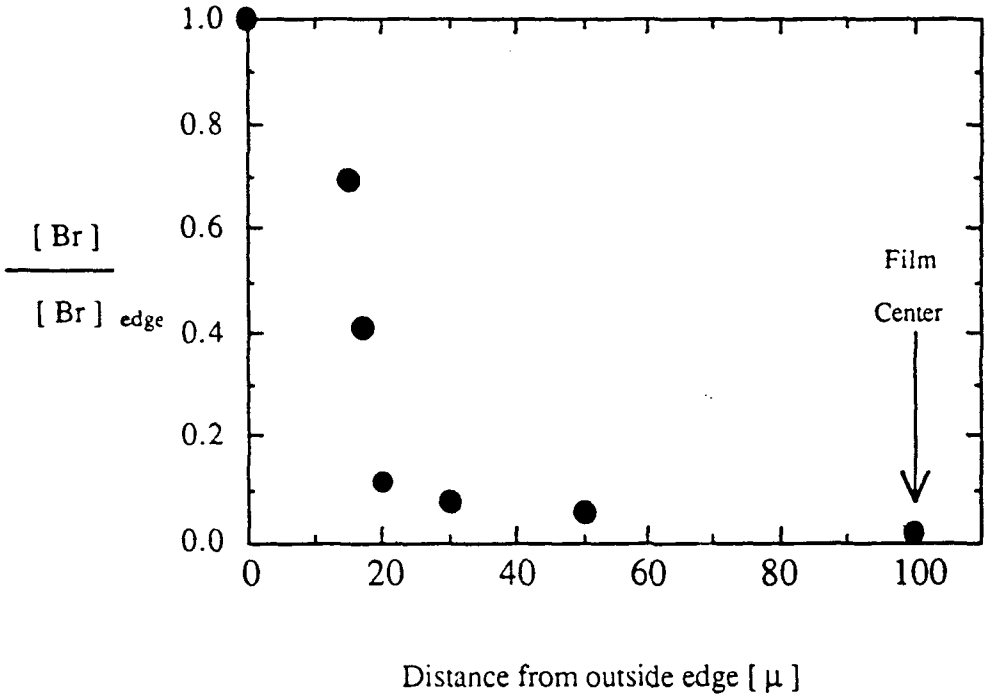

Figure 4-6. Relative Br concentration as a function of distance from the outer edge determined fr ɔm xes. Film center is at 100 μ.

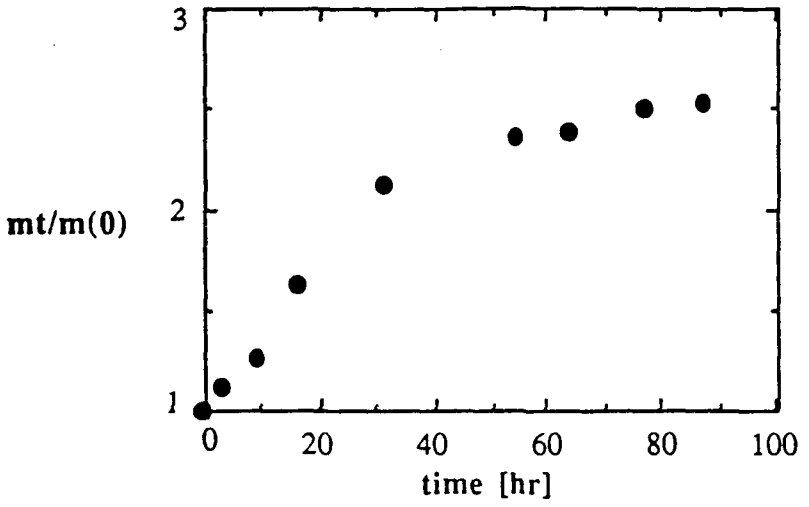

Figure 5.1 Increse in PSPMMA weight as a function of solvent treatment

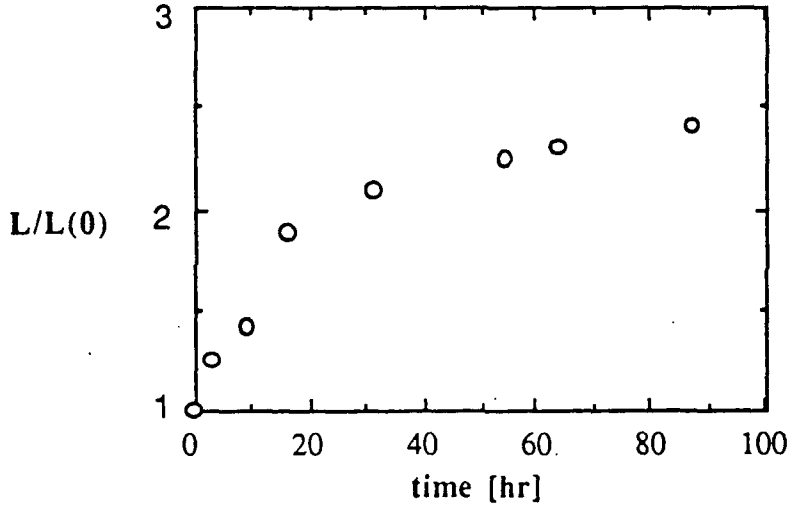

Figure 5.2 Increase in PSPMMA thickness as a function of solvent exposure

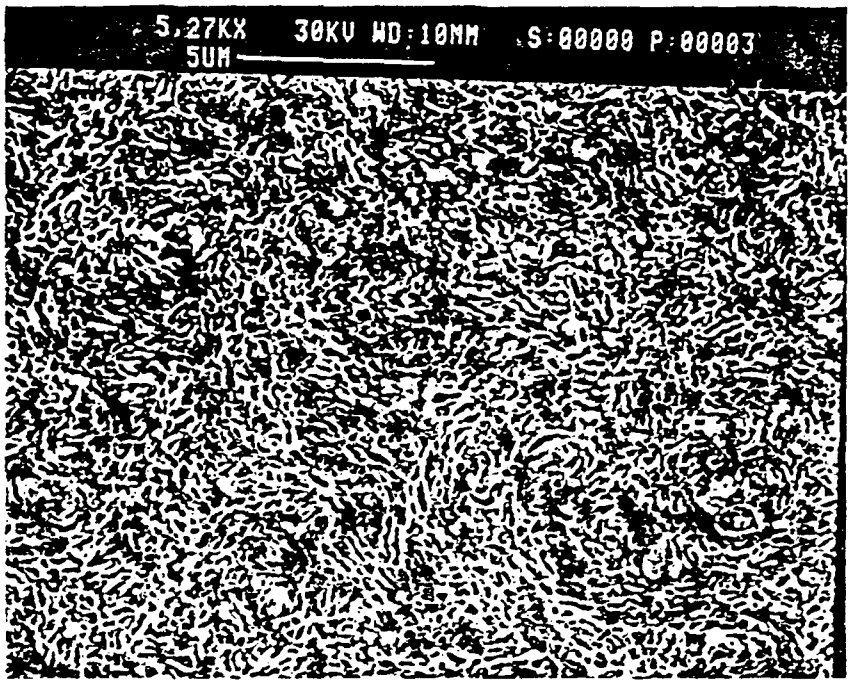

Figure 5-3. SEM surface view of PSPMMA solvent treated to 170% weight increase

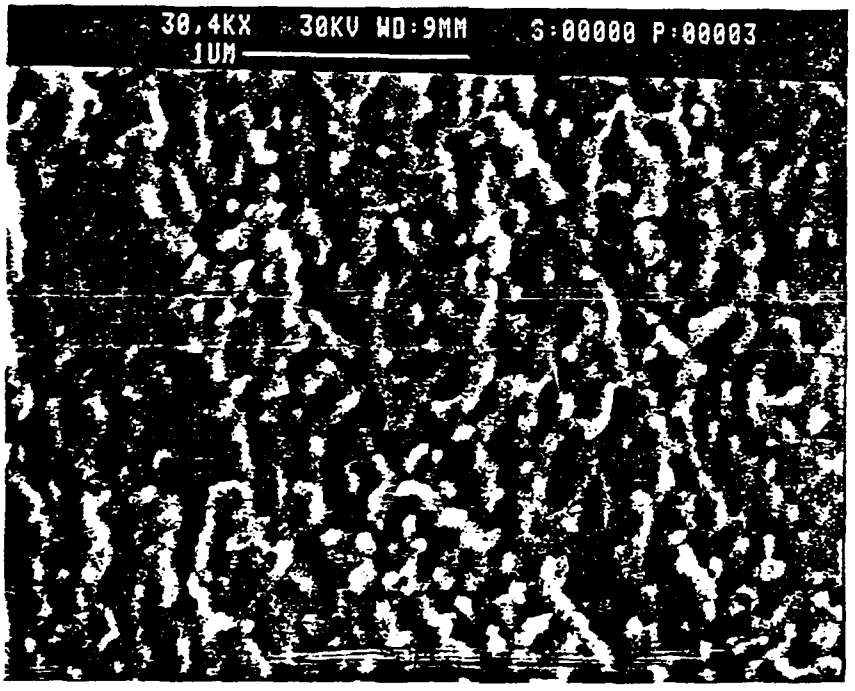

Figure 5-4. SEM edge view of PSPMMA solvent treated to 170% weight increase

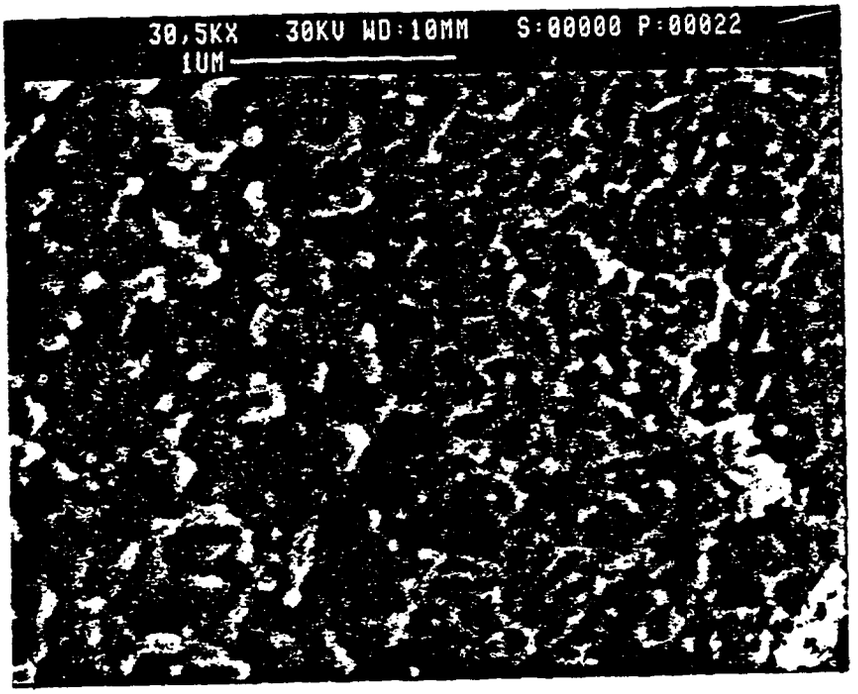

Figure 5-5. SEM edge view of of sharp advancing front in PSPMMA partially solvent treated

Table 2.1
Gas Immobilization Factor in SB

Temp (K)	ß(CO2)	ß(Ar)	ß(CH4)
293	1.9	-	-
298	-	2.3	2.9
323	1.5	1.5	1.6
343	1.3	1.3	1.0
363	1.2	1.0	1.0

Table 3-1
Characterization of PS samples

Polymer	Tg [C]	Mw	Mn
PS1	52	25,600	2,100
PS2	72	26,000	3,000
PS3	91	34,000	5,700
PS4	107	250,000	200,000

Table 3-2

Heats of solution in PS1 and PS4

Gas	Es (PS4)	Es(PS1)	Es*
CO_2	-22.0	-12.1	-10.5
CH_4	-15.7	-4.6	-5.2
Ar	-11.3	-6.2	-5.5

Note: Es* is the heat of solution for all of the PS samples based on the T* temperature scale

Table 5.1
Ideal Separation in Solvent Treated PSPMMA

Solvent treatment % weight increase	Measured $\frac{P(He)}{P(Ar)}$	Measured $\frac{P(CO2)}{P(Ar)}$	Knudsen $\frac{P(He)}{P(Ar)}$	Knudsen $\frac{P(CO2)}{P(Ar)}$
0	15	8.0	3.2	0.6
12	20	5.1	3.2	0.6
18	3.2	0.9	3.2	0.6
43	2.5	0.9	3.2	0.6
75	3.1	0.9	3.2	0.6